Please cite and use: https://doi.org/10.1016/j.ymssp.2020.107168; contact authors if you need a copy.

A Generalized Approach to Anti-Sway Control for Shipboard Cranes

Iain A. Martin[a,*], Rishad A. Irani[a]

[a]Department of Mechanical and Aerospace Engineering, Carleton University, Ottawa, Ontario, K1S 5B6, Canada

ARTICLE INFO

Keywords:
anti-sway control
shipboard crane
gantry crane
knuckle boom crane
nonlinear control
sliding mode control

Abstract

Payload sway for shipboard cranes represents a significant safety concern for deck personnel. In this paper, a generalized trajectory modification strategy is presented that can be applied to a variety of different types of shipboard crane to allow the payload to maintain its desired position with respect to the ship deck in the presence of six degree-of-freedom (DOF) ship motion, and therefore appear stationary to deck personnel. Initially developed for a five DOF shipboard gantry crane, both a de facto proportional-integral-derivative (PID) controller and a sliding mode controller (SMC) are shown in simulation to be successful at tracking the modified trajectory. The PID controller shows a 64% reduction in the root-mean-square-error (RMSE) between the desired and actual payload positions with the addition of the trajectory modifier, and the SMC shows a 74% reduction.

The trajectory modifier is then applied to a six-DOF shipboard knuckle boom crane, with a dynamic model developed to include the mass and inertia of the actuators. The PID controller only shows a 38% reduction in RMSE and struggles to successfully track the trajectory due to the highly nonlinear dynamics of the knuckle boom crane. The SMC controller shows an 82% reduction in RMSE and appears capable of maintaining the desired payload position with the addition of the trajectory modifier.

To further extend the dynamic model of the knuckle boom crane, first-order transfer functions are applied to govern the response of each actuator. A state-of-the-art sliding mode controller is developed to provide stable control of the system, and shows an 84% reduction in RMSE with the addition of the trajectory modifier. The results therefore indicate that trajectory modification is highly effective at dampening payload sway for shipboard cranes, provided a suitable controller can be developed to allow the crane to accurately track the modified trajectory.

PREPRINT

1. Introduction

Precise control of the payload for any crane is an important control problem; unexpected payload motion creates a hazard for anyone working nearby or may cause damage to either the payload itself or the surroundings. However, as cranes are underactuated, nonlinear systems, stable control of the payload can be a challenging task, and has thus attracted significant attention from the research community. In this paper, a generalized approach to anti-sway control for shipboard cranes is presented and applied to both a shipboard gantry crane and a shipboard knuckle boom crane.

In a review published in 2017, Ramli et al. [28] explore the many approaches researchers have taken to improve crane control systems, both shipboard and land-based, to which the reader is referred for a more rigorous overview of crane control strategies. As cranes are nonlinear systems, nonlinear controllers are favored by some researchers as they can often remain effective beyond the operating range of a well tuned, linear controller. A plethora of nonlinear control strategies exist that have been explored by researchers, such as sliding mode control, adaptive control, robust control, fuzzy logic control, and neural networks.

Since 2017 further developments have been made in general crane control, particularly with a focus on neural networks. In 2018, Frikha et al. [6] proposed an adaptive, neuro-sliding mode controller for a planar, three degree-of-freedom (DOF) gantry crane, and showed in simulation the system was able to track a desired trajectory with a varying cable length. Ramli et al. [27] proposed an neural-network based input shaper for a similar three-DOF gantry crane, where the input shaper parameters were tuned in real-time by a neural network, trained with particle swarm optimization. Singh and Agrawal [30] developed a fractional model predictive controller for a two-DOF gantry crane, and Zhang et al. [39] proposed a terminal sliding mode controller that used an observer to estimate disturbances. In

*Corresponding author
IainMartin@cmail.carleton.ca (I.A. Martin); Rishad.Irani@carleton.ca (R.A. Irani)
ORCID(s): 0000-0001-6961-5861 (I.A. Martin); 0000-0003-2854-001X (R.A. Irani)

Please cite and use: https://doi.org/10.1016/j.ymssp.2020.107168; contact authors if you need a copy.

2019, Maghsoudi et al. [17] applied a neural-network based input shaper to a five-DOF gantry crane and showed significant sway reduction.

For shipboard cranes, in addition to the tracking control problem of land-based cranes the crane base itself moves with the ship, further exciting the payload. Particularly in high sea states where deck operations are already dangerous, unexpected payload motion creates a serious hazard. Researchers have taken an interest in shipboard crane control over the past several decades, and have developed several approaches to anti-sway control. In 2001, Henry et al. [8] created a time-delayed feedback controller capable of maintaining a desired ocean-frame (or world-frame) position of the payload for a planar offshore boom crane, and was expanded to a rotary boom crane by Masoud [19]. In 2002, Agostini et al. [1] also developed a control system capable of maintaining the world-frame position of the payload for a rotary boom crane. In 2004, Spathopoulos and Fragopoulos [31] apply a Linear Quadratic Regulator (LQR) to provide anti-sway control for an offshore boom crane.

In 2005, Suthakorn and Parker [34] developed an anti-sway controller for the offshore boom crane, and considered only pitch and yaw motion of the ship. In 2011, Ngo et al. [20] considered a four-DOF container crane and developed an anti-sway controller using a PD controller and a trajectory modifier to maintain the payload's world-frame position, followed by a sliding-mode controller in 2012 [21]. Also in 2012, Fang and Wang [4] considered the planar offshore boom crane and developed controllers to maintain the payload's position with respect to both the world-frame and the deck of the ship using a form of trajectory planning, and provide experimental validation in [5]. In 2013, Ismail and Ha [10] developed a second-order sliding mode controller for the planar offshore boom crane and a rotary boom crane [9]. In 2014, Chu et al. used an energy dissipation method for anti-sway control on a simplified knuckle boom crane, however the crane was not tested with the addition of ship motion [2].

In recent years, the focus of shipboard crane research has been on robust and adaptive controllers. In 2015, Ismail et al. [11] developed a robust sliding mode controller for a planar offshore container crane, designed to handle uncertain disturbances such as wind gusts. Ngo et al. [23, 22] developed a fuzzy-tuned sliding mode controller for a three-DOF offshore container crane, and Qian and Fang [24] developed a nonlinear learning controller for the planar offshore boom crane. In 2017, Qian [25] created an adaptive learning controller for the planar offshore boom crane, and Kim and Park [13] developed a linear controller for a linearized five-DOF container crane. In 2018, Qian [26] developed an adaptive learning controller for the three-DOF container crane, Sun et al. [32] developed an energy-based nonlinear controller for the planar boom crane, and Lu et al. [16] developed a nonlinear controller for the three-DOF boom crane. Both Wang et al. [36] and Tysse and Egeland [35] developed control systems for a simplified model of a shipboard knuckle boom crane, without including the mass and inertia of the hydraulic actuators. In 2019, Sun et al. [33] developed a controller for the three-DOF container crane using an observer to obtain velocity feedback, and Kim and Hong [14] developed an adaptive sliding mode controller for the four-DOF offshore container crane. Yang et al. [37] developed a neural-network based adaptive controller for the planar offshore boom crane, Lu et al. [15] applied nonlinear coordination control to the same planar boom crane. Also in 2019, Martin and Irani [18] investigated various linear and non-linear control strategies for a five-DOF shipboard gantry crane. In 2020, Ramli et al. [29] applied a predictive input shaper to a two-DOF planar overhead crane, and Guo and Chen [7] developed a fault-tolerant fuzzy robust controller for a 2-DOF planar shipboard gantry crane considering roll motion of the ship.

Given the abundance of existing controllers, the objective of this paper is not to propose a new adaptive or robust nonlinear controller for a simplified model of a specific shipboard crane. Rather, the work in this paper builds off the work performed in [18], and seeks to generalize marine crane control by considering more complex dynamic systems than are typically studied, specifically a five-DOF shipboard gantry crane and a six-DOF shipboard knuckle boom crane mounted aboard a ship actuated by full six-DOF ship motion. Both cranes will also incorporate nonlinear characteristics, such as actuator deadzones and saturation.

Therefore, the contribution of this paper to the current state-of-the-art is the development and generalization of marine crane control systems applied to a more realistic dynamic system than is typically studied, and therefore more suitable for real-world applications and deployment. Additionally, given the majority of existing research has focused on maintaining the payload's position with respect to the world frame, this paper will address the control problem of maintaining the payload's position with respect to the ship deck.

Section 2 presents the dynamic model of the five-DOF gantry crane. Both a de facto proportional-integral-derivative (PID) controller and a sliding mode controller (SMC) are implemented to provide anti-sway control in the presence of ship motion, and a generalized trajectory modification strategy presented to improve anti-sway control for the crane. Section 3 presents the dynamic model for the six-DOF knuckle boom crane, where the model includes the masses and inertias of all the major crane components, including the actuators. A first-order transfer function is

PREPRINT

Please cite and use: https://doi.org/10.1016/j.ymssp.2020.107168; contact authors if you need a copy.

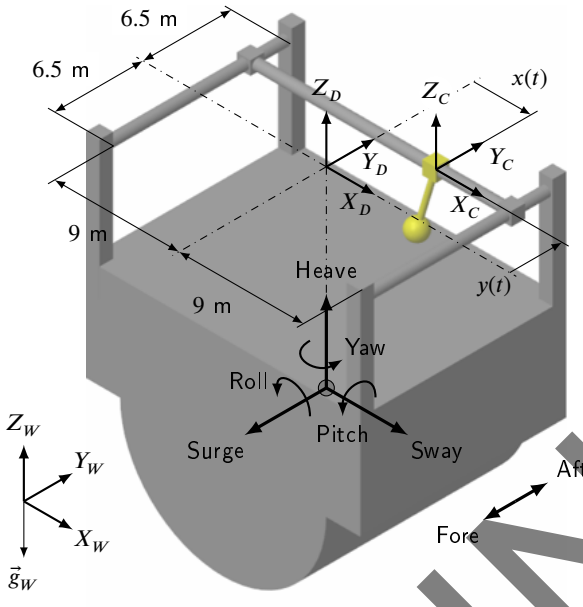

Figure 1: A 3D render of a five-DOF shipboard gantry crane spanning the mission bay of a frigate, generated with MATLAB Simscape.

PREPRINT

also applied to each actuator to simulate actuator dynamics. A de facto PID and a standard SMC are developed that do not compensate for the actuator dynamics, along with a state-of-the-art SMC that accounts for the actuator dynamics. The trajectory modifier is applied and the performance evaluated, and Section 4 presents the conclusions of the work. The equations of motion for the gantry crane are provided in the Appendix, and the equations of motion of the knuckle boom crane are available as MATLAB code.

2. Five-DOF Gantry Crane

A shipboard gantry crane is a common and practical system, with dynamics that are relatively simple compared to other cranes. The gantry crane was simulated using MATLAB Simulink, and Figure 1 shows the 3D render of the crane, intended to represent a cross section of a frigate with an interior gantry crane spanning the mission bay. The ship itself can move with respect to the indicated world frame $(XYZ)_W$ with six degrees of freedom, and Figure 1 shows the positive directions for surge, sway, heave, roll, yaw and pitch. The deck coordinate frame $(XYZ)_D$, where the subscript D denotes "deck", is fixed to the ship at the center of the mission bay, level with the gantry crane cart, and represents the origin for the gantry crane cart. The cart coordinate frame $(XYZ)_C$, where the subscript C denotes "cart", can translate with displacements $x(t)$ and $y(t)$ with respect to $(XYZ)_D$. Note that a positive surge points towards the bow, while the positive Y_W, Y_D and Y_C axes point to the stern. Gravity acts in the negative Z_W axis.

In this paper, the problem considered is to maintain a desired position for the payload with respect to the ship deck coordinate frame $(XYZ)_D$, preventing relative motion of the payload within the mission bay that may cause the payload to collide with either deck personnel or equipment.

2.1. Gantry Crane Equations of Motion

Figure 2 shows the free body diagram of the gantry crane. The cart coordinate frame $(XYZ)_C$ translates with degrees of freedom $x(t)$ and $y(t)$, with motion restricted in the Z_C axis. The cable can be extended to length $l(t)$ below the cart, and the payload can swing with angles $\theta(t)$ and $\phi(t)$ in the $(XZ)_C$ and $(YZ)_C$ planes, respectively.

The five degrees of freedom can be combined into a generalized coordinate vector $\mathbf{q}$,

$$\mathbf{q} = \begin{bmatrix} x(t) & y(t) & l(t) & \theta(t) & \phi(t) \end{bmatrix}^T, \tag{1}$$

and forces $F_x(t)$, $F_y(t)$ and $F_l(t)$ act on the $x(t)$, $y(t)$ and $l(t)$ directions, respectively. Expressed as $\begin{bmatrix} \hat{\imath} & \hat{\jmath} & \hat{k} \end{bmatrix}^T$ vectors

Please cite and use: https://doi.org/10.1016/j.ymssp.2020.107168; contact authors if you need a copy.

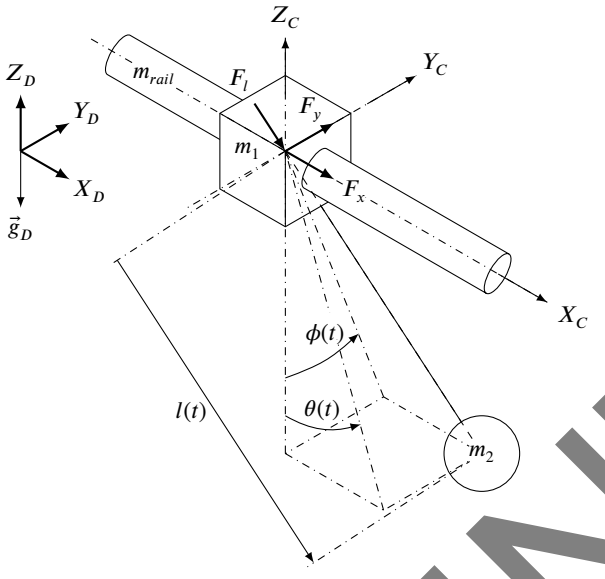

Figure 2: The free body diagram of the five-DOF shipboard gantry crane. The equations of motion were derived with respect to the fixed deck coordinate frame $(XYZ)_D$.

the positions of both the cart and payload are,

$$\vec{p}_{cart} = \begin{bmatrix} x & y & 0 \end{bmatrix}^T, \tag{2}$$

$$\vec{p}_{payload} = \begin{bmatrix} x + l\sin(\theta) \\ y + l\sin(\phi) \\ -l\cos(\theta)\cos(\phi) \end{bmatrix}. \tag{3}$$

For notational simplicity the function of time notation (t) is dropped from all time varying quantities, and any parameters that are constant in time will be specified. The equations of motion were derived using the Lagrange approach consistent with [18], however the gravity vector was rotated into the deck coordinate system $(XYZ)_D$ to determine the potential energies. Using the Tait-Bryan *yaw-pitch-roll* rotation sequence, the world frame gravity vector $\vec{g}_W = \begin{bmatrix} 0 & 0 & g \end{bmatrix}^T$ becomes $\vec{g}_D$,

$$\vec{g}_D = \begin{bmatrix} g\sin(\Theta_r)\cos(\Phi_p) \\ g\sin(\Phi_p) \\ g\cos(\Theta_r)\cos(\Phi_p) \end{bmatrix}, \tag{4}$$

in the deck coordinate frame $(XYZ)_D$, where Θ_r and Φ_p correspond to the ship's roll and pitch angles, respectively. The potential energies of the cart P_{cart} and payload $P_{payload}$ are then

$$P_{cart} = m_{1x} g\sin(\Theta_r)\cos(\Phi_p)x + m_{1y} g\sin(\Phi_p)y \tag{5}$$

$$P_{payload} = m_2 \vec{g}_D^T \cdot \vec{p}_{payload} \tag{6}$$

The equations of motion take the form

$$\begin{bmatrix} M_{11} & M_{12} & M_{13} & M_{14} & M_{15} \\ M_{21} & M_{22} & M_{23} & M_{24} & M_{25} \\ M_{31} & M_{32} & M_{33} & M_{34} & M_{35} \\ M_{41} & M_{42} & M_{43} & M_{44} & M_{45} \\ M_{51} & M_{52} & M_{53} & M_{54} & M_{55} \end{bmatrix} \begin{bmatrix} \ddot{x} \\ \ddot{y} \\ \ddot{l} \\ \ddot{\theta} \\ \ddot{\phi} \end{bmatrix} + \begin{bmatrix} a_1 \\ a_2 \\ a_3 \\ a_4 \\ a_5 \end{bmatrix} = \begin{bmatrix} F_x \\ F_y \\ F_l \\ 0 \\ 0 \end{bmatrix}, \tag{7}$$

PREPRINT

Please cite and use: https://doi.org/10.1016/j.ymssp.2020.107168; contact authors if you need a copy.

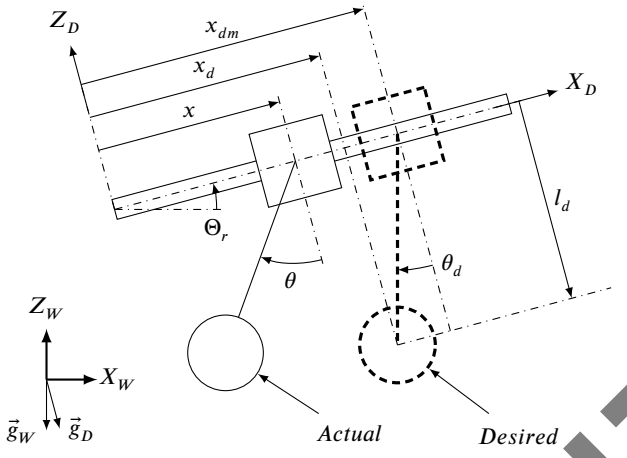

Figure 3: Trajectory modification strategy for the $(XZ)_D$ plane of the shipboard gantry crane. The actual position of the cart and payload is represented by the thin, solid lines, and the desired position of the cart and payload represented by the thick, dashed lines.

or, in a more compact notation,

$$M\ddot{\mathbf{q}} + \mathbf{a} = \mathbf{u}, \tag{8}$$

where $\mathbf{a}$ is a nonlinear vector and $\mathbf{u}$ is a vector of the applied forces. The entries for the mass matrix M and the nonlinear vector $\mathbf{a}$ are provided in Appendix A.

2.2. Trajectory Modification

Noting the last two rows of equation (7), the gantry crane is underactuated and the sway angles of the payload are uncontrollable. However, the natural tendency of the payload is to reach a stable equilibrium with the gravity vector, acting in the negative Z_W direction, a behavior that is exploited in the proposed trajectory modifier.

Consider Figure 3, which illustrates the actual and desired states of the gantry crane in the $(XZ)_D$ plane. In the figure, the ship has rotated about the Y_W axis by a roll angle Θ_r, and the operator has commanded the payload to reach a desired position x_d along the X_D axis. The current, actual position of the cart is x, and the actual sway angle of the payload is θ. To ensure the payload remains at the desired position x_d, the cart can be commanded to reach a position x_{dm}, the modified desired x position, with a desired payload angle of θ_d. The desired distance in the Z_D axis specified by the operator is l_d.

In this paper, it is desired to maintain the payload position relative to the ship deck coordinate frame $(XYZ)_D$. Therefore, the payload is desired to maintain the position x_d, at a distance l_d perpendicular to the gantry rail in order for the payload to appear stationary with respect to any deck personnel. Using a similar approach in the $(YZ)_D$ plane, and measuring the ship's current roll and pitch angles with inclinometers or IMUs, the cart can then be commanded to follow the modified trajectories x_{dm} and y_{dm}

$$x_{dm} = x_d + l_d \tan(\Theta_r), \tag{9}$$

$$y_{dm} = y_d + l_d \tan(\Phi_p), \tag{10}$$

where Θ_r and Φ_p are the ship's current roll and pitch angles, respectively. To maintain the correct z axis position with respect to the deck, the modified cable length l_{dm} is given by

$$l_{dm} = \frac{l_d}{\cos(\Theta_r)\cos(\Phi_p)}. \tag{11}$$

As the payload will naturally attempt to reach a vertical equilibrium with the gravity vector in the $(XYZ)_W$ frame,

PREPRINT

the desired sway angles will correspond to the pitch and roll angles of the ship

$$\theta_d = \Theta_r + \theta_{offset}, \tag{12}$$

$$\phi_d = \Phi_p + \phi_{offset}, \tag{13}$$

where θ_{offset} and ϕ_{offset} are only required to ensure the sway angles are measured with respect to the Z_C axis, see Figure 2. Since for the gantry crane θ and ϕ are measured with respect to the Z_C axis, $\theta_{offset} = \phi_{offset} = 0$. Additionally, depending on the positive direction of the ship's roll and pitch angles the signs of equations (12) and (13) will change to correspond to the positive directions of θ and ϕ shown in Figure 2.

To test the effectiveness of the trajectory modification strategy controllers were developed to allow the gantry crane to track the modified trajectories.

2.3. Controllers for the five-DOF Gantry Crane

The proportional-integral-derivative (PID) controller and sliding mode controller (SMC) developed in [18] were chosen to evaluate the benefits of the trajectory modification strategy.

2.3.1. Proportional-Integral-Derivative (PID) Controller

The PID controller is built using five separate PIDs, each attempting to minimize the error e_{PID} in one of the five degrees of freedom,

$$\mathbf{e_{PID}} = \begin{bmatrix} e_{PID,x} \\ e_{PID,y} \\ e_{PID,l} \\ e_{PID,\theta} \\ e_{PID,\phi} \end{bmatrix} = \begin{bmatrix} x_{dm} - x \\ y_{dm} - y \\ l_{dm} - l \\ \theta_d - \theta \\ \phi_d - \phi \end{bmatrix}. \tag{14}$$

Each PID controller provides a control effort u, corresponding to the degrees of freedom (x, y, l, θ, ϕ). Since the sway angles cannot be directly controlled, the control efforts are combined to incorporate anti-sway action,

$$F_x = \frac{u_x - u_\theta}{2}, \tag{15}$$

$$F_y = \frac{u_y - u_\phi}{2}, \tag{16}$$

$$F_l = u_l. \tag{17}$$

Note the signs in equations (15) and (16) correspond to a θ and ϕ measured as shown in Figure 2.

2.3.2. Sliding Mode Controller (SMC)

The SMC controller uses the equations of motion of the crane to provide the control action. The error vector $\mathbf{e}$ for the SMC is defined with the opposite sign to $\mathbf{e_{PID}}$,

$$\mathbf{e} = -\mathbf{e_{PID}} = \begin{bmatrix} x - x_{dm} \\ y - y_{dm} \\ l - l_{dm} \\ \theta - \theta_d \\ \phi - \phi_d \end{bmatrix}. \tag{18}$$

The sliding surface $\mathbf{s}$ is then defined as

$$\mathbf{s} = \dot{\mathbf{e}} + \lambda \mathbf{e}, \tag{19}$$

where $\lambda = \text{diag}[\lambda_1, \lambda_2, \lambda_3, \lambda_4, \lambda_5]$ is a constant diagonal gain matrix. The derivative of the sliding surface is

$$\dot{\mathbf{s}} = \ddot{\mathbf{e}} + \lambda \dot{\mathbf{e}} = \ddot{\mathbf{q}} - \ddot{\mathbf{q}}_\mathbf{d} + \lambda \dot{\mathbf{e}}. \tag{20}$$

PREPRINT

Please cite and use: https://doi.org/10.1016/j.ymssp.2020.107168; contact authors if you need a copy.

Substituting the equations of motion for the five-DOF gantry crane (8) into (20) gives

$$\dot{\mathbf{s}} = -M^{-1}\mathbf{a} + M^{-1}\mathbf{u} - \ddot{\mathbf{q}}_\mathbf{d} + \lambda\dot{\mathbf{e}}, \tag{21}$$

where setting $\dot{\mathbf{s}} = 0$ gives the control action

$$\mathbf{u} = M\ddot{\mathbf{q}}_\mathbf{d} - M\lambda\dot{\mathbf{e}} + \mathbf{a} - k\text{sat}(\Phi\mathbf{s}), \tag{22}$$

where a robust control term $k\text{sat}(\Phi\mathbf{s})$ is added with constant diagonal gain matricies $k = \text{diag}[k_1, k_2, k_3, k_4, k_5]$ and $\Phi = \text{diag}[\Phi_1, \Phi_2, \Phi_3, \Phi_4, \Phi_5]$. The saturation function is defined as

$$\text{sat}(\Phi\mathbf{s}) = \begin{cases} \Phi\mathbf{s} & \text{if } |\Phi\mathbf{s}| \leq 1 \\ \text{sgn}(\mathbf{s}) & \text{otherwise} \end{cases}. \tag{23}$$

To show the stability of the SMC, consider V_1 as a Lyapunov function candidate,

$$V_1 = \frac{1}{2}\mathbf{s}^T\mathbf{s}, \tag{24}$$

which will be positive definite (p.d) for $\det(\lambda) > 0$. Taking the time derivative of V_1 and noting equation (21) one finds,

$$\dot{V}_1 = \mathbf{s}^T\dot{\mathbf{s}} \tag{25}$$

$$= \mathbf{s}^T\left[-M^{-1}\mathbf{a} + M^{-1}\mathbf{u} - \ddot{\mathbf{q}}_\mathbf{d} + \lambda\dot{\mathbf{e}}\right]. \tag{26}$$

Substitution of the control law $\mathbf{u}$ from (22) into (26) gives

$$\dot{V}_1 = -k\mathbf{s}^T\text{sat}(\Phi\mathbf{s}) \tag{27}$$

For stability, $\dot{V}_1$ must be negative definite (n.d). Note that given the definition of the saturation function provided in equation (23) one can write,

$$|\text{sat}(\Phi\mathbf{s})| \leq |\text{sgn}(\mathbf{s})|, \tag{28}$$

resulting in,

$$\dot{V}_1 \leq -k|\mathbf{s}| < 0. \tag{29}$$

Therefore, if $\det(k) > 0$, $\dot{V}_1$ will be n.d, and by Lyapunov's direct method the SMC is stable.

With the PID and SMC developed to control the gantry crane, the anti-sway performance with the addition of the trajectory modifier could be evaluated.

2.4. Performance with the Modified Trajectory

All simulations were performed in the presence of ship motion generated in ShipMo3D [3] at sea state 6. Table 1 lists the RMS of the ship motion for each degree of freedom. As given in [18], the sea way was modeled with regular waves of the Bretschneider spectrum using a significant wave height of 5 metres and a period of 12.4 seconds. The ship used was the generic frigate included in ShipMo3D, sailing at a speed of 6.000 kt with a heading of 15.0° into the sea. The frequency of the ship's roll, pitch and yaw motion was 0.093 Hz.

The geometric and inertial parameters are provided in Appendix B. A dead-zone of ±100 N and a saturation limit of ±50 kN was placed on each actuator, and all simulations were run at 100 Hz. For all test cases with the gantry crane the desired trajectories for the payload were defined as

$$\dot{x}_d = \dot{y}_d = \begin{cases} 0.3 \text{ m/s} & t < 12 \text{ s} \\ 0 \text{ m/s} & t \geq 12 \text{ s} \end{cases}, \tag{30}$$

PREPRINT

Please cite and use: https://doi.org/10.1016/j.ymssp.2020.107168; contact authors if you need a copy.

Table 1
Ship Motion Parameters

	Surge (m)	Sway (m)	Heave (m)	Roll (°)	Pitch (°)	Yaw (°)
RMS	0.701	0.197	0.908	1.360	1.600	0.244

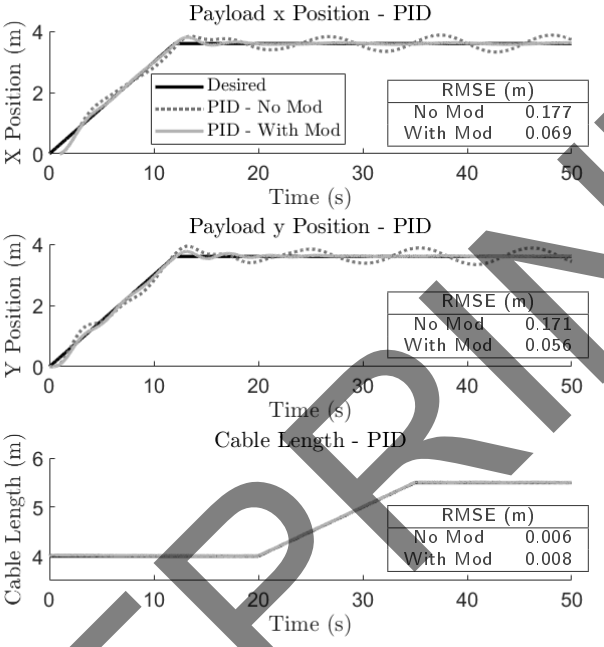

Figure 4: Payload position of the PID controller on the five-DOF gantry crane both with and without the modified trajectories for the cart, where "No Mod" refers to without trajectory modification, while "With Mod" refers to with trajectory modification.

$$\dot{l}_d = \begin{cases} 0 \text{ m/s} & t \le 20 \text{ s} \\ 0.1 \text{ m/s} & 20 < t < 35 \text{ s} \\ 0 \text{ m/s} & t \ge 35 \text{ s} \end{cases}. \tag{31}$$

Each controller was tested both with and without trajectory modification; if trajectory modification was used, each trajectory was modified using equations (9)-(13) before being sent to the each controller. Figures 4 and 5 show the payload position for the PID and SMC controllers, respectively, both with and without trajectory modification. Each figure also provides the root-mean-square-error (RMSE) between the desired payload position x_d, y_d and l_d and the actual payload position, evaluated across the entire duration of each test. The gains for each controller were tuned heuristically to reduce the RMSE while avoiding chatter; the chosen gains are provided in Appendix C.

With the addition of the trajectory modifier the PID controller saw a 64% average reduction in RMSE across the x and y trajectories, while the SMC saw a 73% average reduction. The SMC provides a slight improvement in RMSE over the PID, however unlike the PID the SMC requires the equations of motion of the crane.

Both controllers saw an increase in RMSE for the cable length with the trajectory modification, as with the modifier each controller had to track a more complex trajectory. However, given the cable length RMSEs are all several orders of magnitude below the RMSEs for the x and y trajectories, the performance loss is not considered significant.

PREPRINT

Please cite and use: https://doi.org/10.1016/j.ymssp.2020.107168; contact authors if you need a copy.

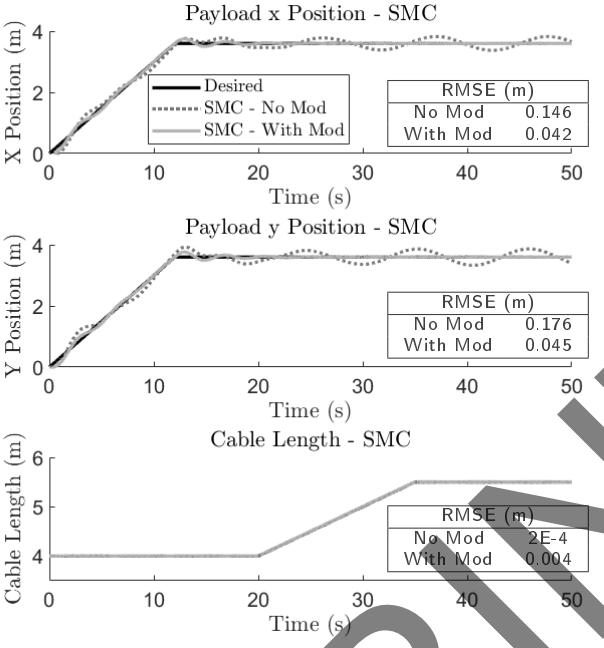

Figure 5: Payload position of the SMC on the five-DOF gantry crane both with and without the modified trajectories for the cart, where "No Mod" refers to without trajectory modification, while "With Mod" refers to with trajectory modification.

PREPRINT

2.5. Generalization of the Trajectory Modification Strategy

Given the effectiveness of simply modifying the cart trajectory in Figures 4 and 5, it is possible other marine cranes can be controlled in a similar way if the coordinates are correctly defined. The strategy can be summarized in three steps:

1. Select a point on the crane that can be considered analogous to the gantry crane cart. The point must be fully actuated.
2. Obtain pitch and roll angular measurements of the ship with inclinometers or IMUs.
3. Using the pitch and roll measurements, control the position of the selected point on the crane using equations (9)-(13).

A six-DOF knuckle boom crane will next be considered to demonstrate the applicability of the trajectory modification strategy.

3. Six-DOF Knuckle Boom Crane

The six-DOF knuckle boom crane was selected as it is both common in industry and has dynamics that are significantly more complex than the five-DOF gantry crane. The masses and inertias of both the hydraulic cylinders and rods are included in the dynamic model. Two cases of the knuckle boom crane will be considered, the first treating the actuators as ideal force sources, and the second including a first-order transfer function for each actuator to model internal dynamics.

3.1. Dynamic Model

Figure 6 shows a render of the knuckle boom crane with the locations of each centre of gravity (CoG), the locations of the applied forces and the location of the deck coordinate frame $(XYZ)_D$. A slew motor rotates the base of the crane with a torque τ_a, and the boom and jib actuators produce forces F_b and F_c, respectively. The winch provides a force F_l to adjust the cable length. The main kinematic chain is comprised of the base with mass m_0, the boom with

Please cite and use: https://doi.org/10.1016/j.ymssp.2020.107168; contact authors if you need a copy.

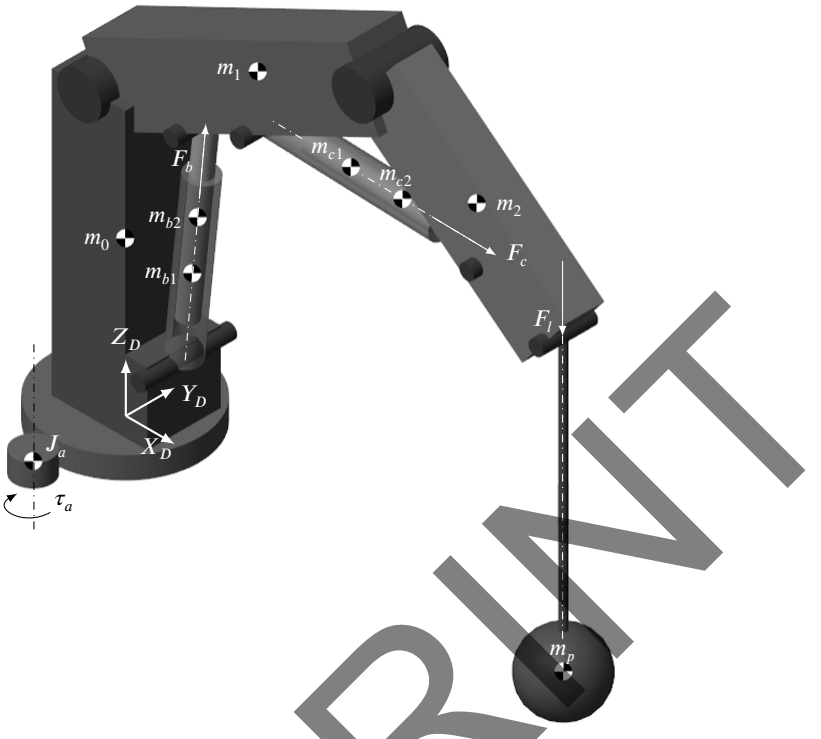

Figure 6: A 3D render of the knuckle boom crane with the locations of each centre of gravity, the applied forces and the deck coordinate frame $(XYZ)_D$.

mass m_1 and the jib with mass m_2. The payload has mass m_p and the slew motor has a mass moment of inertia J_a. The boom actuator is comprised of two components, a cylinder with mass m_{b1} and a rod with mass m_{b2}. Similarly the jib actuator has a cylinder with mass m_{c1} and a rod with mass m_{c2}. Along with a mass, each component has an inertia matrix I located at each CoG.

Figure 7 shows the six degrees of freedom of the knuckle boom crane. The Z_B axis of the base coordinate frame $(XYZ)_B$ can rotate about the Z_D axis of the deck coordinate frame $(XYZ)_D$ by an angle θ_0, actuated by the slew motor. The boom actuator can extend a distance d_1 colinear to the central axis of the cylinder and rod, and likewise the jib actuator can extend a distance d_2. The cable length has a length l_3, and the payload swings with two sway angles θ_3 and θ_4, defined according to the rules of the Denavit-Hartenberg (DH) convention. An additional coordinate frame $(XYZ)_T$ is defined on the tip of the jib, with each axis X_T, Y_T and Z_T parallel to the corresponding deck coordinate frame axes X_D, Y_D and Z_D, respectively. The six degrees of freedom are summarized in the vector $\mathbf{q}$,

$$\mathbf{q} = \begin{bmatrix} \theta_0 & d_1 & d_2 & l_3 & \theta_3 & \theta_4 \end{bmatrix}^T. \tag{32}$$

Figure 8 shows the dimensions needed to fully define the geometry of the knuckle boom crane. The DH method was used to derive the kinematics of the knuckle boom crane, and Figure 9 shows the coordinate frames used in the main kinematic chain. Six coordinate frames are needed to translate from the deck coordinate frame $(XYZ)_D$ to the payload coordinate frame $(XYZ)_6$; coordinate frame $(XYZ)_1$ follows from a $-90°$ rotation about the X_D axis, a translation of l_0 along the Z_D axis, and a rotation θ_0 about the Z_D axis. Coordinate frame $(XYZ)_2$ follows from a rotation θ_1 about the Z_1 axis and a translation l_1 along the X_2 axis. Coordinate frame $(XYZ)_3$ follows from a rotation θ_2 about the Z_2 axis and a translation l_2 along the X_3 axis. A coordinate frame $(XYZ)_4$, not shown in Figure 9, follows from a $90°$ rotation about the X_3 axis and a rotation θ_3 about the Z_3 axis. The coordinate frame $(XYZ)_5$, also not shown follows from a rotation θ_4 about the Z_4 axis, and the final payload coordinate frame $(XYZ)_6$ follows from a translation l_3 along the X_5 axis.

PREPRINT

Please cite and use: https://doi.org/10.1016/j.ymssp.2020.107168; contact authors if you need a copy.

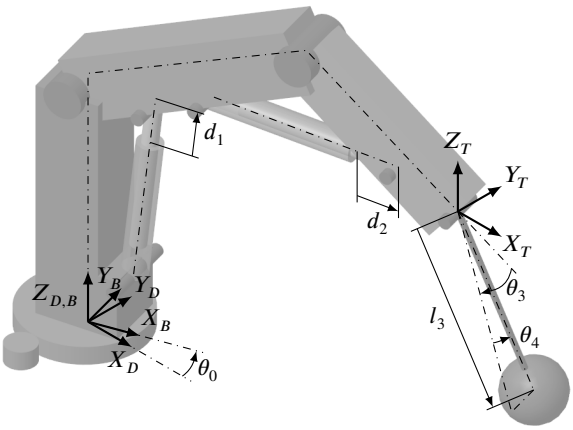

Figure 7: The six degrees of freedom of the knuckle boom crane are the rotation angle of the base θ_0, the actuator extensions d_1 and d_2, the cable length l_3 and the sway angles θ_3 and θ_4.

Therefore, the relationship between the deck coordinate $(XYZ)_D$ and the payload coordinate frame $(XYZ)_6$ can be expressed with a concatenation of transformation matrices,

$$^{D}T_6 = {}^{D}T_1\,{}^{1}T_2\,{}^{2}T_3\,{}^{3}T_4\,{}^{4}T_5\,{}^{5}T_6, \tag{33}$$

where each transformation matrix is fully defined in Appendix D. Note that the angles θ_1 and θ_2 used in the DH derivation can be defined in terms of the actuator extensions using the crane geometry, also given in Appendix D.

Both the boom and jib actuators were given similar DH treatments, and ultimately transformation matrices were derived relating each CoG back to the deck coordinate frame, allowing the equations of motion to be derived using the Lagrange method. The complete derivation is provided in Appendix D. The equations of motion take the form given in equation (8) with a 6×6 mass matrix M, a 6×1 nonlinear vector $\mathbf{a}$ and a 6×1 force vector $\mathbf{u}$.

3.2. Application of the generalized trajectory modification strategy

To apply the proposed trajectory modification strategy the coordinate frame for the tip of the jib $(XYZ)_T$ was chosen to be analogous to the cart coordinate frame $(XYZ)_C$ of the gantry crane. The position of the tip of the jib is fully actuated with the slew motor and the two actuators, completing the first step stated in section 2.5. For the second step, as with the gantry crane pitch and roll measurements of the ship can be obtained using either inclinometers or IMUs.

To complete the third step, a controller must be developed to control the position of the tip coordinate frame. However, the position of $(XYZ)_T$ is typically not directly measured; the feedback measurements obtained from the crane are the slew angle θ_0, the actuator extensions d_1 and d_2, the cable length l_3 and the sway angles of the payload. To obtain the position of the tip from the feedback measurements the forward and inverse kinematics of the crane must be solved.

3.2.1. Forward and Inverse Kinematics

The transformation matrix for the crane tip with respect to the ship deck is

$$^{D}T_3 = {}^{D}T_1\,{}^{1}T_2\,{}^{2}T_3 = \begin{bmatrix} {}^{D}R_3 & {}^{D}\mathbf{r}_3 \\ 0 & 1 \end{bmatrix}, \tag{34}$$

where ${}^{D}R_3$ is a rotation matrix and ${}^{D}\mathbf{r}_3$ a position vector. Evaluating ${}^{D}\mathbf{r}_3$, the x, y and z position of the crane tip with respect to the ship deck is

$$^{D}\mathbf{r}_3 = \begin{bmatrix} x \\ y \\ z \end{bmatrix} = \begin{bmatrix} \cos(\theta_0)\left[l_2\cos(\theta_1+\theta_2)+l_1\cos(\theta_1)\right] \\ \sin(\theta_0)\left[l_2\cos(\theta_1+\theta_2)+l_1\cos(\theta_1)\right] \\ l_0 - l_1\sin(\theta_1) - l_2\sin(\theta_1+\theta_2) \end{bmatrix}. \tag{35}$$

PREPRINT

Please cite and use: https://doi.org/10.1016/j.ymssp.2020.107168; contact authors if you need a copy.

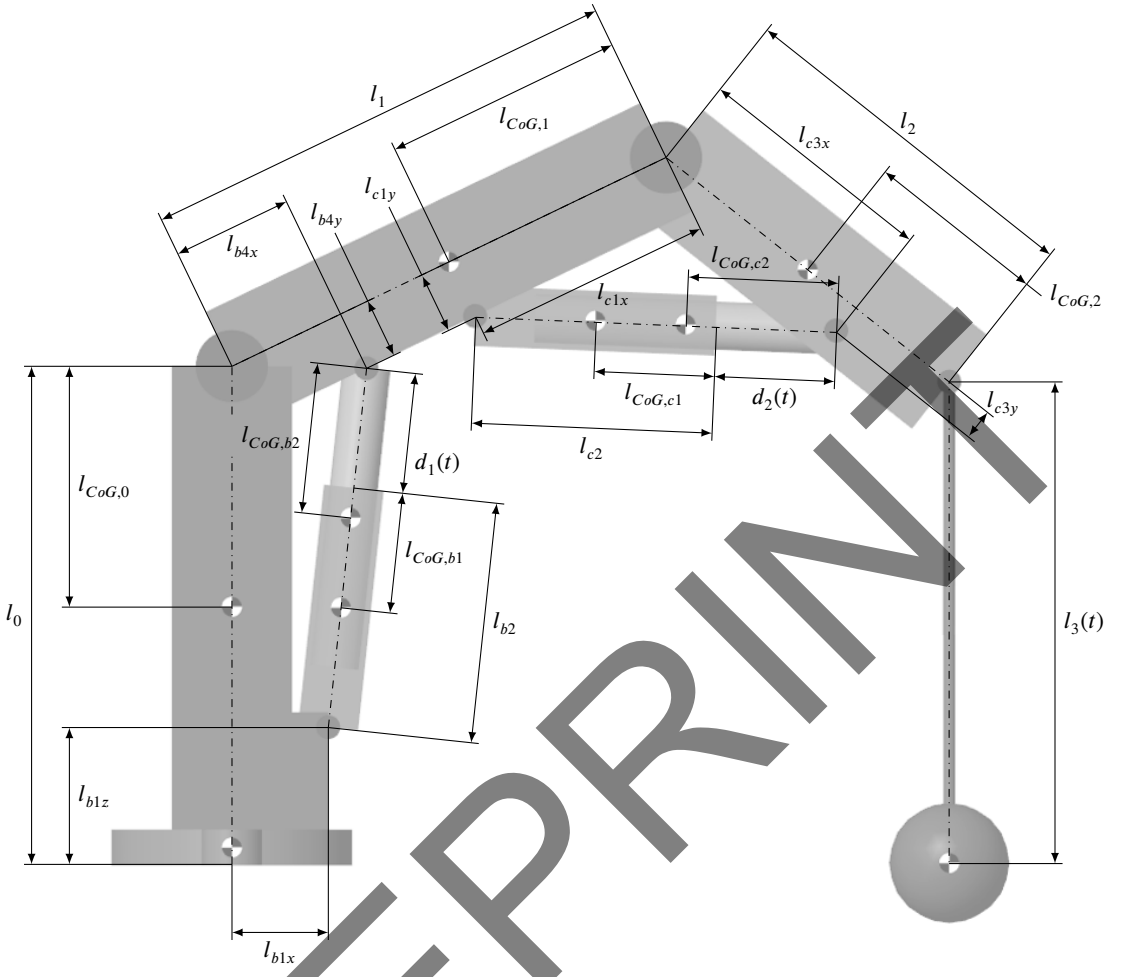

Figure 8: Geometry of the knuckle boom crane. All dimensions are constant in time except for the actuator extensions d_1 and d_2 and the cable length l_3.

If the crane tip is analogous to the cart on the gantry crane, the desired trajectories x_d, y_d and z_d will be specified in terms of the crane tip position. To convert the desired tip position into actuator position setpoints, the inverse kinematic must be solved to express the desired actuator positions $\theta_{0,d}$, $d_{1,d}$ and $d_{2,d}$ in terms of the desired tip positions x_d, y_d and z_d. Solving the system of equations in 35, the inverse kinematic expressions can be derived as

$$\theta_{0,d} = \text{atan2}(y_d, x_d), \tag{36}$$

$$d_{1,d} = \sqrt{a_1^2 + b_1^2 - 2a_1 b_1 \cos(\Gamma_1)} - l_{b2}, \tag{37}$$

$$d_{2,d} = \sqrt{a_2^2 + b_2^2 - 2a_2 b_2 \cos(\Gamma_2)} - l_{c2}, \tag{38}$$

where

$$\alpha = -2l_1 \left[x_d \cos(\theta_{0,d}) + y_d \sin(\theta_{0,d})\right], \tag{39}$$

$$\beta = 2l_1(z_d - l_0), \tag{40}$$

$$\gamma = l_2^2 - l_1^2 - l_0^2 - z_d^2 + 2z_d l_0 - \left[x_d \cos(\theta_{0,d}) + y_d \sin(\theta_{0,d})\right]^2, \tag{41}$$

PREPRINT

Please cite and use: https://doi.org/10.1016/j.ymssp.2020.107168; contact authors if you need a copy.

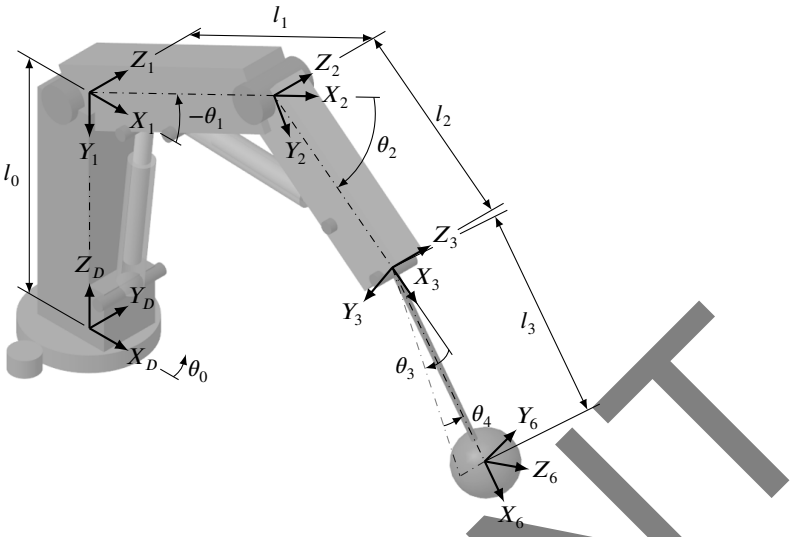

Figure 9: The coordinate frames for the main kinematic chain of the knuckle boom crane.

$$\rho = \sqrt{\alpha^2 + \beta^2}, \tag{42}$$

$$\theta_{1,d} = \text{atan2}\left(\frac{\gamma}{\rho}, -\sqrt{1 - \frac{\gamma^2}{\rho^2}}\right) - \text{atan2}(\alpha, \beta), \tag{43}$$

$$\theta_{2,d} = \text{atan2}\Big[\left(l_0 - l_1 \sin(\theta_{1,d}) - z_d\right), \left(x_d \cos(\theta_{0,d}) + y_d \sin(\theta_{0,d}) - l_1 \cos(\theta_{1,d})\right)\Big] - \theta_{1,d}, \tag{44}$$

$$\Gamma_1 = \frac{\pi}{2} - \theta_{1,d} - \tan^{-1}\left(\frac{l_{b1x}}{l_0 - l_{b1z}}\right) - \tan^{-1}\left(\frac{l_{b4y}}{l_{b4x}}\right), \tag{45}$$

$$\Gamma_2 = \pi - \theta_{2,d} - \tan^{-1}\left(\frac{l_{c1y}}{l_{c1x}}\right) - \tan^{-1}\left(\frac{l_{c3y}}{l_{c3x}}\right) \tag{46}$$

where a_1, a_2, b_1 and b_2 are constant geometric parameters defined in Appendix D and atan2$(\cdot)$ is the four quadrant inverse tangent function.

Therefore as with the gantry crane, equations (9)-(11) can then be used to modify the x, y and l trajectories to account for the ship roll and pitch angles, and each trajectory converted to actuator setpoints using the inverse kinematic relations given in equations (36)-(46). For the z trajectory no modifications are performed, therefore $z_{dm} = z_d$.

3.2.2. Sway Angles for the PID Controller

Instead of using the angles θ_3 and θ_4 for the sway angle measurements, the angles θ and ϕ shown in Figure 10 may be used as they act in the $(XZ)_T$ and $(YZ)_T$ planes, respectively. Using θ and ϕ as the sway angles and measuring the ship's roll and pitch angles *with respect to the deck coordinate frame* $(XYZ)_D$, the trajectory modification equations (12) and (13) can be used to obtain the desired sway angles θ_{dm} and ϕ_{dm} for the PID controller. Note that θ_{offset} and ϕ_{offset} are not required for the PID as both sway angles are measured with respect to the Z_T axis.

3.2.3. Sway Angles for the SMC Controller

For the SMC controller, the equations of motion must be implemented directly to obtain the control law. As a result of using the DH convention to assign the coordinate systems, the sway angles appear in the equations of motion as θ_3 and θ_4, not θ and ϕ. Therefore, to apply trajectory modification to the sway angles for the SMC, the ship roll and pitch angles must be measured *with respect to the rotating base coordinate frame* $(XYZ)_B$, illustrated in Figure 7.

PREPRINT

Please cite and use: https://doi.org/10.1016/j.ymssp.2020.107168; contact authors if you need a copy.

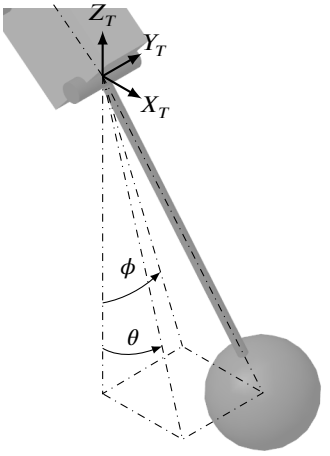

Figure 10: Sway angles θ and ϕ measured with respect to the tip coordinate frame $(XYZ)_T$.

Additionally, θ_3 must be corrected by the offset

$$\theta_{3,offset} = \frac{\pi}{2} - \theta_1 - \theta_2, \tag{47}$$

to align $\theta_3 = 0°$ with the vertical direction. Therefore, for the SMC the modified trajectories $\theta_{3,dm}$ and $\theta_{4,dm}$ are

$$\theta_{3,dm} = \Theta_r + \theta_{3,offset} \tag{48}$$

$$\theta_{4,dm} = \Phi_p. \tag{49}$$

No offset is required for $\theta_{4,dm}$ as it is already measured with respect to the correct axis.

3.3. Control System Overview

Figure 11 presents an overview of the knuckle boom crane control system, where $\mathbf{x_d}$ is the vector of desired payload positions with respect to the ship deck, $\mathbf{x_{dm}}$ is the vector of modified desired trajectories and $\mathbf{q_{dm}}$ is the vector of desired trajectories converted to slew angle and actuator extensions using the inverse kinematics, equations (36)-(46). The control action $\mathbf{u}$ is computed at the actuator level, and the measured states of the crane $\mathbf{q}$ converted to deck coordinates $\mathbf{x}$ using equation (35). For the SMC, each vector is defined as

$$\mathbf{x_d} = \begin{bmatrix} x_d & y_d & z_d & l_{3,d} & \theta^*_{3,dm} & \theta^*_{4,dm} \end{bmatrix}^T, \tag{50}$$

$$\mathbf{x_{dm}} = \begin{bmatrix} x_{dm} & y_{dm} & z_{dm} & l_{3,dm} & \theta^*_{3,dm} & \theta^*_{4,dm} \end{bmatrix}^T, \tag{51}$$

$$\mathbf{q_{dm}} = \begin{bmatrix} \theta_{0,dm} & d_{1,dm} & d_{2,dm} & l_{3,dm} & \theta^*_{3,dm} & \theta^*_{4,dm} \end{bmatrix}^T, \tag{52}$$

$$\mathbf{u} = \begin{bmatrix} \tau_a & F_b & F_c & F_l & 0 & 0 \end{bmatrix}^T, \tag{53}$$

$$\mathbf{q} = \begin{bmatrix} \theta_0 & d_1 & d_2 & l_3 & \theta^*_3 & \theta^*_4 \end{bmatrix}^T, \tag{54}$$

$$\mathbf{x} = \begin{bmatrix} x & y & z & l_3 & \theta^*_3 & \theta^*_4 \end{bmatrix}^T, \tag{55}$$

where * denotes variables that change if using the PID controller; for the PID, θ and θ_{dm} replace θ^*_3 and $\theta^*_{3,dm}$, respectively, while ϕ and ϕ_{dm} replace θ^*_4 and $\theta^*_{4,dm}$, respectively.

3.4. PID Controller

As with the five-DOF gantry crane a separate PID controller is used to control each degree of freedom. The PID error vector for the knuckle boom crane is the errors in each actuator setpoint, as well as the errors in the sway angles

PREPRINT

Please cite and use: https://doi.org/10.1016/j.ymssp.2020.107168; contact authors if you need a copy.

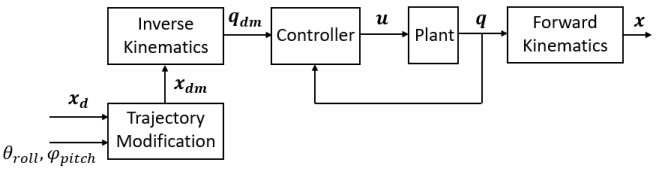

Figure 11: High level schematic of the knuckle boom crane control system.

θ and ϕ:

$$\mathbf{e_{PID}} = \begin{bmatrix} e_{PID,\theta 0} \\ e_{PID,d1} \\ e_{PID,d2} \\ e_{PID,l3} \\ e_{PID,\theta} \\ e_{PID,\phi} \end{bmatrix} = \begin{bmatrix} \theta_{0,dm} - \theta_0 \\ d_{1,dm} - d_1 \\ d_{2,dm} - d_2 \\ l_{3,dm} - l_3 \\ \theta_{dm} - \theta \\ \phi_{dm} - \phi \end{bmatrix}. \tag{56}$$

The inverse kinematic relations given in equations (36)-(46) are used to convert $e_{PID,\theta}$ and $e_{PID,\phi}$ to errors at the actuator level, where $e_{PID,\theta}$ is assumed to be an error in the X_T axis and $e_{PID,\phi}$ an error in the Y_T axis. It is assumed there is no error in the Z_T axis. Mapping the sway angle errors to the actuator level, $e_{PID,\theta}$ and $e_{PID,\phi}$ are replaced with errors $e_{PID,\theta,\theta 0}$, $e_{PID,\theta,d1}$ and $e_{PID,\theta,d2}$.

Therefore, seven PID controllers are used to compute control actions corresponding to $e_{PID,\theta 0}$, $e_{PID,d1}$, $e_{PID,d2}$, and $e_{PID,l3}$, as well as $e_{PID,\theta,\theta 0}$, $e_{PID,\theta,d1}$ and $e_{PID,\theta,d2}$, resulting in control actions $u_{\theta 0}$, u_{d1}, u_{d2}, u_{l3}, $u_{\theta,\theta 0}$, $u_{\theta,d1}$ and $u_{\theta,d2}$. The control actions are then be combined to provide the final actuator forces,

$$\mathbf{u} = \begin{bmatrix} \tau_a \\ F_b \\ F_c \\ F_l \\ 0 \\ 0 \end{bmatrix} = \begin{bmatrix} \frac{u_{\theta 0} + u_{\theta,\theta 0}}{2} \\ \frac{u_{d1} + u_{\theta,d1}}{2} \\ \frac{u_{d2} + u_{\theta,d2}}{2} \\ u_{l3} \\ 0 \\ 0 \end{bmatrix}. \tag{57}$$

As the PID controller is a linear controller, a nonlinear SMC was also developed to evaluate any improvement in tracking performance.

3.5. Sliding Mode Controller (Without Actuator Dynamics)

The SMC derived in this section will be referred to as the *ideal* SMC, as it does not include any compensation for additional actuator dynamics.

The *ideal* SMC was built assuming each actuator had no internal dynamics, and that each force could be treated as an ideal force source, as was the case for the gantry crane. Therefore, since the equations of motion of the knuckle boom crane take the same form as for the gantry crane, the sliding control laws could be derived in an identical way, giving

$$\mathbf{u} = M\ddot{\mathbf{q}}_\mathbf{d} - M\lambda\dot{\mathbf{e}} + \mathbf{a} - k\,\mathrm{sat}\,(\Phi\mathbf{s}), \tag{58}$$

where $\lambda = \mathrm{diag}[\lambda_1, \lambda_2, \lambda_3, \lambda_4, \lambda_5, \lambda_6]$, $k = \mathrm{diag}[k_1, k_2, k_3, k_4, k_5, k_6]$ are constant gain matrices, and the SMC error

PREPRINT

Please cite and use: https://doi.org/10.1016/j.ymssp.2020.107168; contact authors if you need a copy.

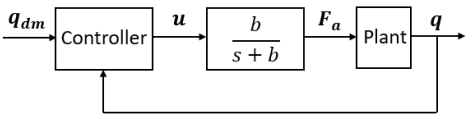

Figure 12: The addition of the actuator dynamics into the crane control system.

vector $\mathbf{e}$ is given by

$$\mathbf{e} = \begin{bmatrix} \theta_0 - \theta_{0,dm} \\ d_1 - d_{1,dm} \\ d_2 - d_{2,dm} \\ l_3 - l_{3,dm} \\ \theta_3 - \theta_{3,dm} \\ \theta_4 - \theta_{4,dm} \end{bmatrix}. \tag{59}$$

Note that since the sliding control law takes the same form as for the gantry crane, for which the SMC was shown to be stable, the SMC for the knuckle boom crane will also be stable.

In order to provide stable control with the inclusion of actuator dynamics, the *compensated* SMC was developed.

3.6. Sliding Mode Controller (Including Actuator Dynamics)

The SMC derived in this section will be referred to as the *compensated* SMC, as it includes compensation for the additional actuator dynamics. It was developed using a backstepping procedure inspired by the work of Yao in [38].

To enhance the accuracy of the dynamic model, a first-order transfer function was applied to govern the response of each actuator,

$$\frac{F_i(s)}{U_i(s)} = \frac{b_i}{s + b_i}, \tag{60}$$

where s is the Laplace variable and F_i the force or torque applied by actuator i on the crane, corresponding to $F_1 = \tau_a$, $F_2 = F_b$, $F_3 = F_c$ and $F_4 = F_l$. $U_i(s)$ is the control effort supplied by the controller, and $b_i > 0$ is a constant. Figure 12 shows the actuator dynamics inserted into the control system shown in Figure 11, where $\mathbf{F_a} = [F_1, F_2, F_3, F_4, 0, 0]^T$.

To ensure the SMC remains stable with the addition of the actuator dynamics the control law must be updated. Converting equation (60) into state-space form,

$$\dot{\boldsymbol{\gamma}} = -b\boldsymbol{\gamma} + \mathbf{u}, \tag{61}$$

$$\mathbf{F_a} = b\boldsymbol{\gamma}, \tag{62}$$

where $\boldsymbol{\gamma}$ is the new state vector and $b = \text{diag}[b_1, b_2, b_3, b_4, b_5, b_6]$. Consider the sliding function $\mathbf{s_1}$ such that $\mathbf{s_1} = \mathbf{s}$, with $\mathbf{s}$ defined in equation 19. The time derivative $\dot{\mathbf{s}}_\mathbf{1}$ of $\mathbf{s_1}$ is

$$\dot{\mathbf{s}}_\mathbf{1} = M^{-1}\mathbf{u_v} - M^{-1}\mathbf{a} - \ddot{\mathbf{q}}_\mathbf{d} + \lambda\dot{\mathbf{e}}, \tag{63}$$

where $\mathbf{u_v}$ is a virtual control action,

$$\mathbf{u_v} = \mathbf{F_a} + \mathbf{u_1} \tag{64}$$

$$= b\boldsymbol{\gamma} + \mathbf{u_1}, \tag{65}$$

where

$$\boldsymbol{\gamma} = b^{-1}\left(M\ddot{\mathbf{q}}_\mathbf{d} - M\lambda\dot{\mathbf{e}} + \mathbf{a}\right), \tag{66}$$

PREPRINT

Please cite and use: https://doi.org/10.1016/j.ymssp.2020.107168; contact authors if you need a copy.

and $\mathbf{u_1}$ is the robust control action given by

$$\mathbf{u_1} = -k_\alpha \text{sat}\left(\Phi_\alpha \mathbf{s_1}\right), \tag{67}$$

where $k_\alpha = \text{diag}[k_{\alpha,1}, k_{\alpha,2}, k_{\alpha,3}, k_{\alpha,4}, k_{\alpha,5}, k_{\alpha,6}]$ and $\lambda_\alpha = \text{diag}[\lambda_{\alpha,1}, \lambda_{\alpha,2}, \lambda_{\alpha,3}, \lambda_{\alpha,4}, \lambda_{\alpha,5}, \lambda_{\alpha,6}]$ are constant gain matrices.

We define a second error variable $\mathbf{s_2} = -\mathbf{u_1} = \mathbf{F_a} - \mathbf{u_v}$. Considering equation (61), the time derivative $\dot{\mathbf{s}}_\mathbf{2}$ of $\mathbf{s_2}$ is given by

$$\dot{\mathbf{s}}_\mathbf{2} = \dot{\mathbf{F}}_\mathbf{a} - \dot{\mathbf{u}}_\mathbf{v} \tag{68}$$

$$= b\dot{\boldsymbol{\gamma}} - \left(b\dot{\boldsymbol{\gamma}} + \dot{\mathbf{u}}_\mathbf{1}\right) \tag{69}$$

$$= b\left(-b\boldsymbol{\gamma} + \mathbf{u}\right) - b\dot{\boldsymbol{\gamma}} - \dot{\mathbf{u}}_\mathbf{1}. \tag{70}$$

Setting $\dot{\mathbf{s}}_\mathbf{2} = 0$ and solving for the control action $\mathbf{u}$,

$$\mathbf{u} = \dot{\boldsymbol{\gamma}} + b\boldsymbol{\gamma} + b^{-1}\dot{\mathbf{u}}_\mathbf{1} + \mathbf{u_2}, \tag{71}$$

where $\mathbf{u_2}$ is a second robust control action,

$$\mathbf{u_2} = -k_\beta \text{sat}\left(\Phi_\beta \mathbf{s_2}\right), \tag{72}$$

where $k_\beta = \text{diag}[k_{\beta,1}, k_{\beta,2}, k_{\beta,3}, k_{\beta,4}, k_{\beta,5}, k_{\beta,6}]$ and $\lambda_\beta = \text{diag}[\lambda_{\beta,1}, \lambda_{\beta,2}, \lambda_{\beta,3}, \lambda_{\beta,4}, \lambda_{\beta,5}, \lambda_{\beta,6}]$ are again constant gain matrices. The p.d Lyapunov function is defined as

$$V_2 = \frac{1}{2}\mathbf{s_1}^T\mathbf{s_1} + \frac{1}{2}\mathbf{s_2}^T\mathbf{s_2}. \tag{73}$$

Following substitution of the control laws, the time derivative $\dot{V}_2$ simplifies to

$$\dot{V}_2 = \mathbf{s_1}^T\mathbf{u_1} + \mathbf{s_2}^T\mathbf{u_2}, \tag{74}$$

where, by the same logic provided in section 2.3.2,

$$\dot{V}_2 \leq -k_\alpha|\mathbf{s_1}| - k_\beta|\mathbf{s_2}|. \tag{75}$$

Since $\dot{V}_2$ is n.d, the control system is stable by Lyapunov's direct method.

3.7. Simulation Results

All simulations were run at 100 Hz. The desired trajectories for the payload were selected as

$$\dot{x}_d = \dot{y}_d = \begin{cases} 0.1 \text{ m/s} & t < 12 \text{ s} \\ 0 \text{ m/s} & t \geq 12 \text{ s} \end{cases}, \tag{76}$$

$$\dot{z}_d = \begin{cases} 0.2 \text{ m/s} & t < 12 \text{ s} \\ 0 \text{ m/s} & t \geq 12 \text{ s} \end{cases}, \tag{77}$$

$$\dot{l}_d = \begin{cases} 0 \text{ m/s} & t \leq 20 \text{ s} \\ 0.1 \text{ m/s} & 20 < t < 35 \text{ s} \\ 0 \text{ m/s} & t \geq 35 \text{ s} \end{cases}. \tag{78}$$

Note that the initial position of the payload, x_0, y_0 and z_0 corresponds to the position of the payload with actuator rest positions $\theta_0 = 0°$, $d_1 = d_2 = 0.5$ m and an initial cable length $l_3 = 4$ m. Additionally, for all tests a dead-zone of ±100 N was placed on each actuator, along with saturation limits of ±50 kNm for the slew motor, ±500 kN for the boom actuator, ±100 kN for the jib actuator and ±100 kN for the winch motor.

PREPRINT

Please cite and use: https://doi.org/10.1016/j.ymssp.2020.107168; contact authors if you need a copy.

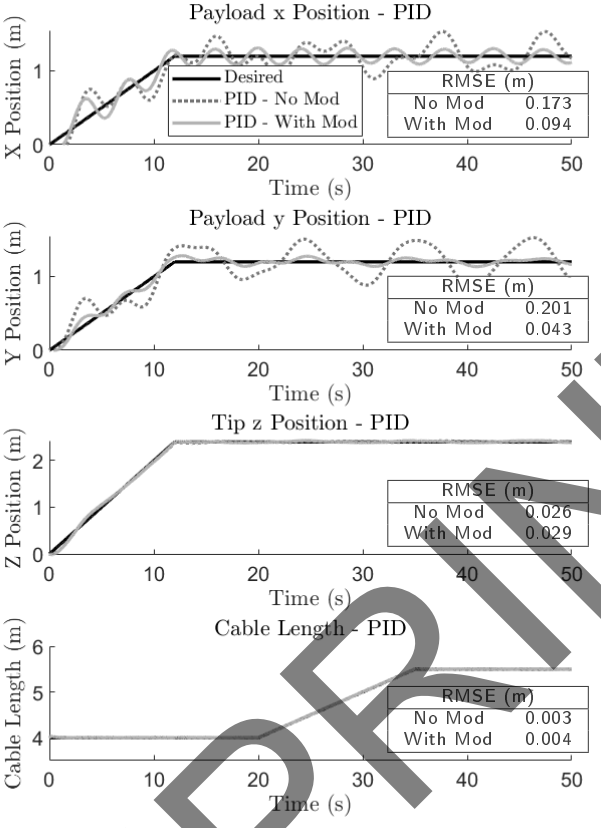

Figure 13: Tracking performance of the PID controller for the knuckle boom crane without additional actuator dynamics, both with and without the trajectory modifier.

PREPRINT

The same ship motion data was used as in the gantry crane tests, corresponding to sea state 6. The gains used in the simulations were tuned heurstically to reduce the RMSE and avoid chattering (provided in Appendix C).

3.7.1. Performance without the Actuator Dynamics

Figure 13 shows the trajectory tracking performance of the PID controller without the actuator dynamics, both with and without the addition of the trajectory modifier. While the trajectory modifier provides an average reduction in RMSE of 38% across the x, y and z trajectories, the PID struggles to follow the modified trajectory due to the nonlinear dynamics of the knuckle boom crane.

Figure 14 shows the trajectory tracking performance of the *ideal* SMC without the actuator dynamics, both with and without the trajectory modifier. The trajectory modifier provides an average reduction in RMSE of 82% across the x, y and z trajectories, demonstrating the superior performance of the SMC over the PID at maintaining the payload's position with respect to the ship deck.

3.7.2. Performance with Actuator Dynamics

Figure 15 shows the performance of the *compensated* SMC controller derived in Section 3.6 with the first-order transfer functions applied to each actuator and $b_i = 10$, corresponding to a time constant of 0.1 seconds. Both the PID controller and the *ideal* SMC were found to be unstable with the addition of the actuator dynamics. The *compensated* SMC however was stable and saw an average reduction in RMSE of 84% across the x, y and z trajectories with the addition of the trajectory modifier. The results indicate actuator dynamics must be considered to ensure the design of

Please cite and use: https://doi.org/10.1016/j.ymssp.2020.107168; contact authors if you need a copy.

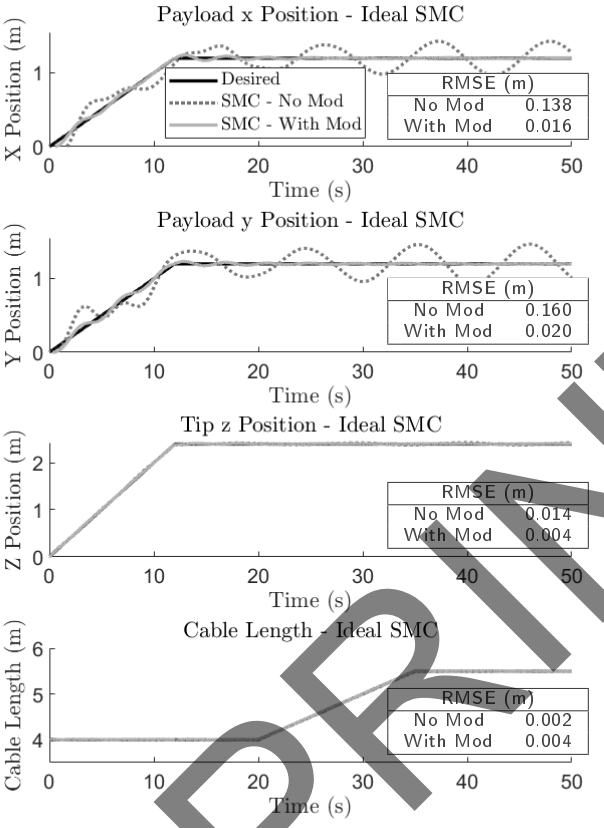

Figure 14: Tracking performance of the *ideal* SMC controller for the knuckle boom crane without additional actuator dynamics, both with and without the trajectory modifier.

a stable controller.

4. Conclusion

In this paper, a generalized control strategy given in equations (9)-(13) was developed that allows a crane with a suitable controller to provide anti-sway control when mounted aboard a ship. The approach of the generalized control strategy is to modify the desired trajectories specified by the operator using the ship's roll and pitch angles, measured from either IMUs or inclinometers. The modified trajectories exploit the payload's natural tendency to reach a stable equilibrium with the gravity vector, and provided a suitable controller is used to control the crane the payload will appear to remain stationary with respect to the ship deck in the presence of ship motion. The trajectory modifier was generalized to allow deployment to various marine cranes.

Initially developed for a five-DOF shipboard gantry crane, both a PID and SMC were successfully used to track the modified trajectory, showing a 64% and 74% reduction in RMSE between the desired and actual payload positions with the use of the trajectory modifier. Applying the generalized trajectory modifier to a six-DOF knuckle boom crane, the SMC was again successful at tracking the modified trajectory showing an 82% reduction in RMSE. The PID only showed a 38% reduction for the knuckle boom crane and struggled to track the modified trajectory due to the nonlinear dynamics of the knuckle boom crane.

To model actuator dynamics, first-order transfer functions were applied to each actuator. A stable SMC was derived to control the system with the addition of the actuator dynamics and showed an 84% reduction in RMSE with the addition of the trajectory modifier.

PREPRINT

Please cite and use: https://doi.org/10.1016/j.ymssp.2020.107168; contact authors if you need a copy.

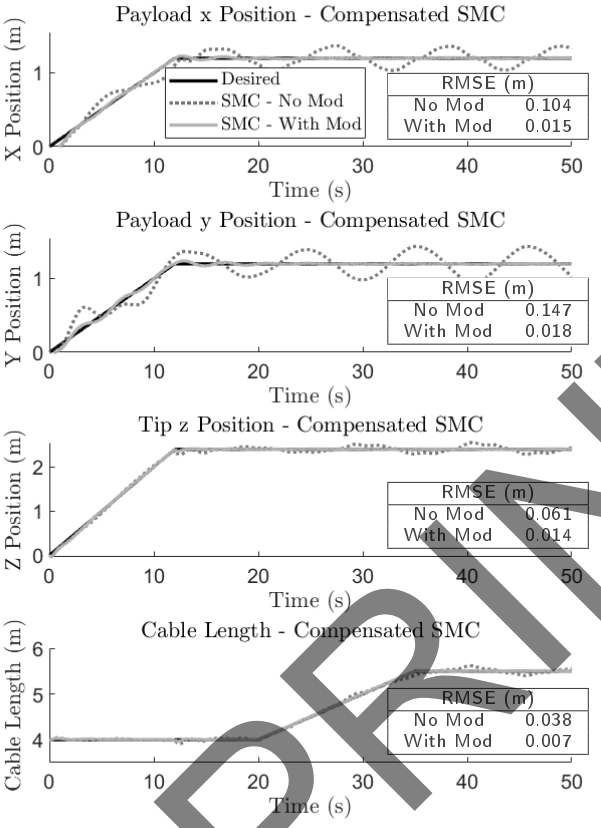

Figure 15: Tracking performance of the *compensated* SMC with the addition of actuator dynamics, both with and without trajectory modification.

The results show that if a controller can be built that allows a shipboard crane to successfully track the modified trajectory, the crane can be made to maintain the payload at the desired position relative to the ship deck. The requirement on the controller is that it allows the crane to accurately track the modified trajectory; for the gantry crane, either a linear PID or the nonlinear SMC were sufficient at tracking the trajectory, whereas for the knuckle boom crane only the SMC could accurately track the trajectory.

Acknowledgment

The authors acknowledge the support of the Natural Sciences and Engineering Research Council of Canada (NSERC), [funding reference number 06967]. Cette recherche a été financée par le Conseil de recherches en sciences naturelles et en génie du Canada (CRSNG), [numéro de référence 06967]. Additionally, we would like to acknowledge Kraken Robotic Systems Inc. for their feedback in the work, and Carleton University for their support. The authors would like to thank DSA LTD (Dynamic Systems Analysis Ltd) for the in-kind donation of ShipMo3D.

A. Gantry Crane Equations of Motion

The entries for the equations of motion of the gantry crane are

$$M_{11} = m_{1x} + m_2 \tag{79}$$

$$M_{22} = m_{1y} + m_2 \tag{80}$$

PREPRINT

Please cite and use: https://doi.org/10.1016/j.ymssp.2020.107168; contact authors if you need a copy.

$$M_{33} = m_2\Big[\cos^2(\theta)\cos^2(\phi) - \cos^2(\theta) - 2\cos^2(\phi)\Big] \tag{81}$$

$$M_{44} = -m_2 l^2\Big[\left(\cos^2(\phi) - 1\right)\cos^2(\theta) - \cos^2(\phi)\Big] \tag{82}$$

$$M_{55} = -m_2 l^2\Big[\left(\cos^2(\phi) - 1\right)\cos^2(\theta) - \cos^2(\phi)\Big] \tag{83}$$

$$M_{13} = M_{31} = m_2\sin(\theta) \tag{84}$$

$$M_{14} = M_{41} = m_2 l\cos(\theta) \tag{85}$$

$$M_{23} = M_{32} = m_2\sin(\phi) \tag{86}$$

$$M_{25} = M_{52} = m_2 l\cos(\phi) \tag{87}$$

$$M_{34} = M_{43} = m_2 l\cos(\theta)\sin(\theta)\sin^2(\phi) \tag{88}$$

$$M_{35} = M_{53} = m_2 l\cos(\phi)\sin(\phi)\sin^2(\theta) \tag{89}$$

$$M_{45} = M_{54} = m_2 l^2\cos(\phi)\cos(\theta)\sin(\phi)\sin(\theta) \tag{90}$$

$$M_{12} = M_{21} = M_{15} = M_{51} = M_{24} = M_{42} = 0 \tag{91}$$

and

$$a_1 = 2m_2\dot{l}\dot{\theta}\cos(\theta) - m_2 l\dot{\theta}^2\sin(\theta) + g(m_{1x} + m_2)\sin(\Theta_r)\cos(\Phi_p) \tag{92}$$

$$a_2 = 2m_2\dot{l}\dot{\phi}\cos(\phi) - m_2 l\dot{\phi}^2\sin(\phi) - g(m_{1y} + m_2)\sin(\Phi_p) \tag{93}$$

$$\begin{aligned} a_3 = {} & -m_2\Big[l\left(\dot{\phi}^2 + \dot{\theta}^2\right)\cos^2(\phi) + 2\dot{l}\dot{\phi}\cos(\phi)\sin(\phi) \\ & - l\dot{\theta}^2\Big]\cos^2(\theta) + \Big[-2m_2\dot{l}\dot{\theta}\sin(\theta)\cos^2(\phi) \\ & + \Big[2m_2 l\dot{\theta}\dot{\phi}\sin(\theta)\sin(\phi) \\ & - m_2 g\cos(\Theta_r)\cos(\Phi_p)\Big]\cos(\phi) \\ & + 2m_2\dot{l}\dot{\theta}\sin(\theta)\Big]\cos(\theta) + m_2 l\dot{\phi}^2\cos^2(\phi) \\ & + 2m_2\dot{l}\dot{\phi}\sin(\phi)\cos(\phi) \\ & + m_2 g\sin(\theta)\sin(\Theta_r)\cos(\Phi_p) \\ & - m_2 g\sin(\phi)\sin(\Phi_p) - m_2 l\left(\dot{\theta}^2 + \dot{\phi}^2\right) \end{aligned} \tag{94}$$

$$\begin{aligned} a_4 = {} & \Big[-2m_2 l\dot{l}\dot{\theta}\cos^2(\theta) + m_2 l^2\left(\dot{\theta}^2 + \dot{\phi}^2\right)\cos(\theta)\sin(\theta) \\ & + 2m_2 l\dot{l}\dot{\theta}\Big]\cos^2(\phi) + m_2 l\Big[-2l\dot{\theta}\dot{\phi}\sin(\phi) \\ & + g\cos(\Theta_r)\cos(\Phi_p)\sin(\theta) \\ & + 2\dot{l}\dot{\phi}\cos(\theta)\sin(\theta)\sin(\phi) \\ & + 2l\dot{\theta}\dot{\phi}\cos^2(\theta)\sin(\phi)\Big]\cos(\phi) + m_2 l\Big[2\dot{l}\dot{\theta}\cos^2(\theta) \end{aligned}$$

PREPRINT

Please cite and use: https://doi.org/10.1016/j.ymssp.2020.107168; contact authors if you need a copy.

Table 2
Gantry Crane Model Parameters

Parameter	Value
m_1	5000 kg
m_{rail}	10000 kg
m_2	1770 kg
l_0	4.00 m

$$- l\dot{\theta}^2 \cos(\theta)\sin(\theta) + g\cos(\theta)\sin(\Theta_r)\cos(\Phi_p)\Big] \tag{95}$$

$$\begin{aligned} a_5 = m_2 l\Big[& -2\dot{l}\dot{\phi}\cos^2(\theta) + 2\dot{l}\dot{\phi} \\ & + 2l\dot{\theta}\dot{\phi}\cos(\theta)\sin(\theta)\Big]\cos^2(\phi) \\ & + \Big[m_2 l^2\left(\dot{\theta}^2 + \dot{\phi}^2\right)\cos^2(\theta)\sin(\phi) \\ & + 2m_2 l\dot{l}\dot{\theta}\cos(\theta)\sin(\theta)\sin(\phi) \\ & + m_2 l\Big[-g\sin(\Phi_p) - l\dot{\phi}^2\sin(\phi)\Big]\Big]\cos(\phi) \\ & + m_2 l\Big[g\cos(\theta)\sin(\phi)\cos(\Theta_r)\cos(\Phi_p) \\ & - 2l\dot{\phi}\dot{\theta}\cos(\theta)\sin(\theta) + 2\dot{l}\dot{\phi}\cos^2(\theta)\Big] \end{aligned} \tag{96}$$

B. Model Parameters

Tables 2 and 3 provide the model parameters used in the simulations for the gantry and knuckle boom cranes, respectively. For the gantry crane, the y axis will have a total mass of both the mass of the cart and mass of the rail, $m_{1y} = m_1 + m_{rail}$, while for the x axis $m_{1x} = m_1$. The payload for both cranes was considered to be a small Zodiac-style watercraft [40].

C. Controller Gains

Tables 4 and 5 provide the gains used for the gantry crane PID and SMC controllers, respectively. Tables 6 and 7 provide the gains used for the knuckle boom crane PID and *ideal* SMC controllers, respectively, during tests without the additional actuator dynamics. Table 8 provides the gains for the *compensated* SMC used with the additional actuator dynamics.

D. Knuckle Boom Crane Equations of Motion

D.1. Knuckle Boom Crane Kinematics

The Denavit–Hartenberg method was used to derive the kinematics of the knuckle boom crane, as outlined in [12]. Note for notational simplicity, (t) will be dropped from all time varying quantities, and $\sin(x)$ and $\cos(x)$ may be abbreviated $s(x)$ and $c(x)$. Figure 8 presents the dimensions used in the derivation.

D.1.1. Main Kinematic Chain

Figure 9 shows the coordinate frames for the main kinematic chain, with DH parameters listed in Table 9. The origin frame is the coordinate frame $(XYZ)_D$, fixed to the ship deck.

PREPRINT

Please cite and use: https://doi.org/10.1016/j.ymssp.2020.107168; contact authors if you need a copy.

Table 3
Knuckle Boom Crane Model Parameters

Geometric		Inertial	
Parameter	Value	Parameter	Value
l_0	4 m	m_0	5000 kg
l_1	4 m	m_1	3000 kg
l_2	2 m	m_2	2000 kg
$l_{b1,x}$	0.8 m	m_p	1770 kg
$l_{b1,z}$	1 m	$m_{b1} = m_{c1}$	1000 kg
$l_{b4,x}$	1 m	$m_{b2} = m_{c2}$	1000 kg
$l_{b4,y}$	0.5 m	$I_{xx,0}$	7083.33 kgm^2
$l_{c1,x}$	2 m	$I_{yy,0}$	833.33 kgm^2
$l_{c1,y}$	0.5 m	$I_{zz,0}$	7083.33 kgm^2
$l_{c3,x}$	2 m	$I_{xx,1}$	390.625 kgm^2
$l_{c3,y}$	0.5 m	$I_{yy,1}$	4140.63 kgm^2
l_{b2}	2 m	$I_{zz,1}$	4250.00 kgm^2
l_{c2}	2 m	$I_{xx,2}$	208.333 kgm^2
$l_{CoG,b1}$	1 m	$I_{yy,2}$	1541.67 kgm^2
$l_{CoG,b2}$	1.25 m	$I_{zz,2}$	1666.67 kgm^2
$l_{CoG,c1}$	1 m	J_a	3.125 kgm^2
$l_{CoG,c2}$	1.25 m	$I_{xx,b1} = I_{xx,c1}$	40 kgm^2
N	4	$I_{yy,b1} = I_{yy,c1}$	900 kgm^2
		$I_{zz,b1} = I_{zz,c1}$	900 kgm^2
		$I_{xx,b2} = I_{xx,c2}$	10 kgm^2
		$I_{yy,b1} = I_{yy,c1}$	650 kgm^2
		$I_{zz,b1} = I_{zz,c1}$	650 kgm^2

Table 4
Gantry Crane PID Controller Gains

$K_{P,x}$	1.65E5	$K_{I,x}$	0	$K_{D,x}$	3E5
$K_{P,y}$	1E5	$K_{I,y}$	0	$K_{D,y}$	2E6
$K_{P,l}$	1E6	$K_{I,l}$	1E5	$K_{D,l}$	1E5
$K_{P,\theta}$	1E6	$K_{I,\theta}$	0	$K_{D,\theta}$	0
$K_{P,\phi}$	1E6	$K_{I,\phi}$	0	$K_{D,\phi}$	0

Table 5
Gantry Crane SMC Controller Gains

λ_1	5	k_1	1E5	Φ_1	1
λ_2	5	k_2	1E5	Φ_2	1
λ_3	5	k_3	1E5	Φ_3	1
λ_4	50	k_4	0	Φ_4	0
λ_5	50	k_5	0	Φ_5	0

The transformation matrices for the main chain, as well as for the centres of gravity of the base, boom and jib are

$$ {}^{D}T_1 = \begin{bmatrix} c(\theta_0) & 0 & -s(\theta_0) & 0 \\ s(\theta_0) & 0 & c(\theta_0) & 0 \\ 0 & -1 & 0 & l_0 \\ 0 & 0 & 0 & 1 \end{bmatrix}, \tag{97} $$

PREPRINT

Please cite and use: https://doi.org/10.1016/j.ymssp.2020.107168; contact authors if you need a copy.

Table 6
Knuckle Boom Crane PID Controller Gains

$K_{P,x}$	3E6	$K_{I,x}$	3E5	$K_{D,x}$	3E6
$K_{P,y}$	5E6	$K_{I,y}$	5E6	$K_{D,y}$	5E6
$K_{P,z}$	3E5	$K_{I,z}$	1E5	$K_{D,z}$	3E5
$K_{P,l}$	5E5	$K_{I,l}$	1E6	$K_{D,l}$	5E4
$K_{P,\theta 1}$	1E5	$K_{I,\theta 1}$	0	$K_{D,\theta 1}$	0
$K_{P,\theta 2}$	5E5	$K_{I,\theta 2}$	0	$K_{D,\theta 2}$	0
$K_{P,\theta 3}$	1E5	$K_{I,\theta 3}$	0	$K_{D,\theta 3}$	0

Table 7
Knuckle Boom Crane *Ideal* SMC Controller Gains

λ_1	20	k_1	1E8	Φ_1	100
λ_2	20	k_2	1E8	Φ_2	100
λ_3	20	k_3	1E7	Φ_3	100
λ_4	20	k_4	1E6	Φ_4	100
λ_5	20	k_5	0	Φ_5	0
λ_6	20	k_6	0	Φ_6	0

Table 8
Knuckle Boom Crane *Compensated* SMC Controller Gains

λ_1	20	$k_{\alpha,1}$	5E5	$\Phi_{\alpha,1}$	10	$k_{\beta,1}$	1E5	$\Phi_{\beta,1}$	1E4
λ_2	20	$k_{\alpha,2}$	5E5	$\Phi_{\alpha,2}$	10	$k_{\beta,2}$	1E4	$\Phi_{\beta,2}$	1E3
λ_3	20	$k_{\alpha,3}$	1E5	$\Phi_{\alpha,3}$	10	$k_{\beta,3}$	1E4	$\Phi_{\beta,3}$	1E3
λ_4	20	$k_{\alpha,4}$	5E3	$\Phi_{\alpha,4}$	1	$k_{\beta,4}$	1E3	$\Phi_{\beta,4}$	1E3
λ_5	20	$k_{\alpha,5}$	0	$\Phi_{\alpha,5}$	0	$k_{\beta,5}$	0	$\Phi_{\beta,5}$	0
λ_6	20	$k_{\alpha,6}$	0	$\Phi_{\alpha,6}$	0	$k_{\beta,6}$	0	$\Phi_{\beta,6}$	0

Table 9
DH Table - Main Chain

	$\mathbf{a_i}$	α_i	$\mathbf{d_i}$	θ_i
1	0	$-90°$	l_0	θ_0
2	l_1	0	0	θ_1
3	l_2	0	0	θ_2
4	0	$90°$	0	θ_3
5	0	0	0	θ_4
6	l_3	0	0	0

$$ {}^1T_2 = \begin{bmatrix} c(\theta_1) & -s(\theta_1) & 0 & l_1 c(\theta_1) \\ s(\theta_1) & c(\theta_1) & 0 & l_1 s(\theta_1) \\ 0 & 0 & 1 & 0 \\ 0 & 0 & 0 & 1 \end{bmatrix}, \tag{98} $$

$$ {}^2T_3 = \begin{bmatrix} c(\theta_2) & -s(\theta_2) & 0 & l_2 c(\theta_2) \\ s(\theta_2) & c(\theta_2) & 0 & l_2 s(\theta_2) \\ 0 & 0 & 1 & 0 \\ 0 & 0 & 0 & 1 \end{bmatrix}, \tag{99} $$

PREPRINT

Please cite and use: https://doi.org/10.1016/j.ymssp.2020.107168; contact authors if you need a copy.

$$ {}^{3}T_{4} = \begin{bmatrix} c(\theta_3) & 0 & s(\theta_3) & 0 \\ s(\theta_3) & 0 & -c(\theta_3) & 0 \\ 0 & 1 & 0 & 0 \\ 0 & 0 & 0 & 1 \end{bmatrix}, \tag{100} $$

$$ {}^{4}T_{5} = \begin{bmatrix} c(\theta_4) & -s(\theta_4) & 0 & 0 \\ s(\theta_4) & c(\theta_4) & 0 & 0 \\ 0 & 0 & 1 & 0 \\ 0 & 0 & 0 & 1 \end{bmatrix}, \tag{101} $$

$$ {}^{5}T_{6} = \begin{bmatrix} 1 & 0 & 0 & l_3 \\ 0 & 1 & 0 & 0 \\ 0 & 0 & 1 & 0 \\ 0 & 0 & 0 & 1 \end{bmatrix}, \tag{102} $$

$$ {}^{1}T_{CoG,0} = \begin{bmatrix} 1 & 0 & 0 & 0 \\ 0 & 1 & 0 & l_{CoG,0} \\ 0 & 0 & 1 & 0 \\ 0 & 0 & 0 & 1 \end{bmatrix} \tag{103} $$

$$ {}^{2}T_{CoG,1} = \begin{bmatrix} 1 & 0 & 0 & -l_{CoG,1} \\ 0 & 1 & 0 & 0 \\ 0 & 0 & 1 & 0 \\ 0 & 0 & 0 & 1 \end{bmatrix}, \tag{104} $$

$$ {}^{3}T_{CoG,2} = \begin{bmatrix} 1 & 0 & 0 & -l_{CoG,2} \\ 0 & 1 & 0 & 0 \\ 0 & 0 & 1 & 0 \\ 0 & 0 & 0 & 1 \end{bmatrix}. \tag{105} $$

Therefore, the transformation matrices to the payload frame ${}^{0}T_{6}$ and the centres of mass for the base, boom and jib with respect to the origin frame are simply concatenations of the above transformation matrices,

$$ {}^{D}T_{6} = \begin{bmatrix} {}^{D}\boldsymbol{R}_{6} & {}^{D}\mathbf{r}_{6} \\ 0 & 1 \end{bmatrix} = {}^{D}T_{1}\,{}^{1}T_{2}\,{}^{2}T_{3}\,{}^{3}T_{4}\,{}^{4}T_{5}\,{}^{5}T_{6}, \tag{106} $$

$$ {}^{D}T_{CoG,0} = \begin{bmatrix} {}^{D}R_{CoG,0} & {}^{D}\mathbf{r}_{CoG,0} \\ 0 & 1 \end{bmatrix} = {}^{D}T_{1}\,{}^{1}T_{CoG,0}, \tag{107} $$

$$ {}^{D}T_{CoG,1} = \begin{bmatrix} {}^{D}R_{CoG,1} & {}^{D}\mathbf{r}_{CoG,1} \\ 0 & 1 \end{bmatrix} = {}^{D}T_{1}\,{}^{1}T_{2}\,{}^{2}T_{CoG,1}, \tag{108} $$

$$ \begin{aligned} {}^{D}T_{CoG,2} &= \begin{bmatrix} {}^{D}R_{CoG,2} & {}^{D}\mathbf{r}_{CoG,2} \\ 0 & 1 \end{bmatrix} \\ &= {}^{D}T_{1}\,{}^{1}T_{2}\,{}^{2}T_{3}\,{}^{3}T_{CoG,2}, \end{aligned} \tag{109} $$

where R is the rotation matrix and $\mathbf{r}$ the position vector. The velocity matrices of the payload and each CoG can then be calculated,

$$ {}^{D}V_{6} = \begin{bmatrix} {}^{D}\tilde{\omega}_{6} & {}^{D}\mathbf{v}_{6} \\ 0 & 1 \end{bmatrix} = {}^{D}\dot{T}_{6}\,{}^{D}T_{6}^{-1}, \tag{110} $$

$$ {}^{D}V_{CoG,0} = \begin{bmatrix} {}^{D}\tilde{\omega}_{CoG,0} & {}^{D}\mathbf{v}_{CoG,0} \\ 0 & 1 \end{bmatrix} = {}^{D}\dot{T}_{CoG,0}\,{}^{D}T_{CoG,0}^{-1}, \tag{111} $$

$$ {}^{D}V_{CoG,1} = \begin{bmatrix} {}^{D}\tilde{\omega}_{CoG,1} & {}^{D}\mathbf{v}_{CoG,1} \\ 0 & 1 \end{bmatrix} = {}^{D}\dot{T}_{CoG,1}\,{}^{D}T_{CoG,1}^{-1}, \tag{112} $$

$$ {}^{D}V_{CoG,2} = \begin{bmatrix} {}^{D}\tilde{\omega}_{CoG,2} & {}^{D}\mathbf{v}_{CoG,2} \\ 0 & 1 \end{bmatrix} = {}^{D}\dot{T}_{CoG,2}\,{}^{D}T_{CoG,2}^{-1}, \tag{113} $$

PREPRINT

Please cite and use: https://doi.org/10.1016/j.ymssp.2020.107168; contact authors if you need a copy.

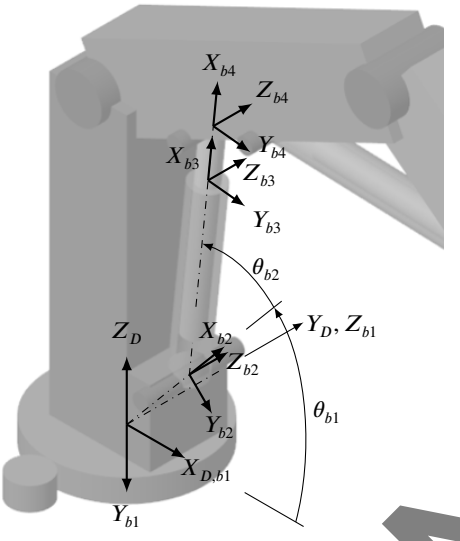

Figure 16: The coordinate frames for the boom actuator kinematic chain of the knuckle boom crane.

Table 10
DH Table - Boom Actuator

	$\mathbf{a_i}$	$\alpha_\mathbf{i}$	$\mathbf{d_i}$	$\theta_\mathbf{i}$
b_1	0	$-90°$	0	θ_0
b_2	l_{b1}	0	0	$-\theta_{b1}$
b_3	l_{b2}	0	0	$-\theta_{b2}$
b_4	l_{b3}	0	0	0

where $\tilde{\omega}$ is the skew symmetric velocity matrix and $\mathbf{v}$ the translational velocity vector.

D.1.2. Boom Actuator Kinematic Chain

Figure 16 shows the coordinate frames for the boom actuator kinematic chain, corresponding to the DH parameters listed in Table 10.

The transformation matrices for the boom actuator kinematic chain are then given by,

$$ {}^{D}T_{b1} = \begin{bmatrix} c(\theta_0) & 0 & -s(\theta_0) & 0 \\ s(\theta_0) & 0 & c(\theta_0) & 0 \\ 0 & -1 & 0 & 0 \\ 0 & 0 & 0 & 1 \end{bmatrix}, \tag{114} $$

$$ {}^{b1}T_{b2} = \begin{bmatrix} c(-\theta_{b1}) & -s(-\theta_{b1}) & 0 & l_{b1}c(-\theta_{b1}) \\ s(-\theta_{b1}) & c(-\theta_{b1}) & 0 & l_{b1}s(-\theta_{b1}) \\ 0 & 0 & 1 & 0 \\ 0 & 0 & 0 & 1 \end{bmatrix}, \tag{115} $$

$$ {}^{b2}T_{b3} = \begin{bmatrix} c(-\theta_{b2}) & -s(-\theta_{b2}) & 0 & l_{b2}c(-\theta_{b2}) \\ s(-\theta_{b2}) & c(-\theta_{b2}) & 0 & l_{b2}s(-\theta_{b2}) \\ 0 & 0 & 1 & 0 \\ 0 & 0 & 0 & 1 \end{bmatrix}, \tag{116} $$

PREPRINT

Please cite and use: https://doi.org/10.1016/j.ymssp.2020.107168; contact authors if you need a copy.

Table 11
DH Table - Jib Actuator

	$\mathbf{a_i}$	α_i	$\mathbf{d_i}$	θ_i
c_1	l_{c1}	0	0	θ_{c1}
c_2	l_{c2}	0	0	θ_{c2}
c_3	l_{c3}	0	0	0

$$ {}^{b3}T_{b4} = \begin{bmatrix} 1 & 0 & 0 & d_1 \\ 0 & 1 & 0 & 0 \\ 0 & 0 & 1 & 0 \\ 0 & 0 & 0 & 1 \end{bmatrix}, \tag{117} $$

$$ {}^{b3}T_{CoG,b1} = \begin{bmatrix} 1 & 0 & 0 & -l_{CoG,b1} \\ 0 & 1 & 0 & 0 \\ 0 & 0 & 1 & 0 \\ 0 & 0 & 0 & 1 \end{bmatrix}, \tag{118} $$

$$ {}^{b4}T_{CoG,b2} = \begin{bmatrix} 1 & 0 & 0 & -l_{CoG,b2} \\ 0 & 1 & 0 & 0 \\ 0 & 0 & 1 & 0 \\ 0 & 0 & 0 & 1 \end{bmatrix}, \tag{119} $$

and concatenating the transformation matrices to relate the motion of each CoG to the origin,

$$ \begin{aligned} {}^{D}T_{CoG,b1} &= \begin{bmatrix} {}^{D}R_{CoG,b1} & {}^{D}\mathbf{r}_{CoG,b1} \\ 0 & 1 \end{bmatrix} \\ &= {}^{D}T_{b1}\,{}^{b1}T_{b2}\,{}^{b2}T_{b3}\,{}^{b3}T_{CoG,b1}, \end{aligned} \tag{120} $$

$$ \begin{aligned} {}^{D}T_{CoG,b2} &= \begin{bmatrix} {}^{D}R_{CoG,b2} & {}^{D}\mathbf{r}_{CoG,b2} \\ 0 & 1 \end{bmatrix} \\ &= {}^{D}T_{b1}\,{}^{b1}T_{b2}\,{}^{b2}T_{b3}\,{}^{b3}T_{b4}\,{}^{b4}T_{CoG,b2}. \end{aligned} \tag{121} $$

The velocity matrices for the boom actuator are then

$$ \begin{aligned} {}^{D}V_{CoG,b1} &= \begin{bmatrix} {}^{D}\tilde{\omega}_{CoG,b1} & {}^{D}\mathbf{v}_{CoG,b1} \\ 0 & 1 \end{bmatrix} \\ &= {}^{D}\dot{T}_{CoG,b1}\,{}^{D}T^{-1}_{CoG,b1}, \end{aligned} \tag{122} $$

$$ \begin{aligned} {}^{D}V_{CoG,b2} &= \begin{bmatrix} {}^{D}\tilde{\omega}_{CoG,b2} & {}^{D}\mathbf{v}_{CoG,b2} \\ 0 & 1 \end{bmatrix} \\ &= {}^{D}\dot{T}_{CoG,b2}\,{}^{D}T^{-1}_{CoG,b2}. \end{aligned} \tag{123} $$

D.1.3. Jib Actuator Kinematic Chain

Figure 17 shows the coordinate frames for the jib actuator kinematic chain, corresponding to the DH parameters listed in Table 11.

The transformation matrices for the jib actuator kinematic chain are then,

$$ {}^{1}T_{c1} = \begin{bmatrix} c(\theta_{c1}) & -s(\theta_{c1}) & 0 & l_{c1}c(\theta_{c1}) \\ s(\theta_{c1}) & c(\theta_{c1}) & 0 & l_{c1}s(\theta_{c1}) \\ 0 & 0 & 1 & 0 \\ 0 & 0 & 0 & 1 \end{bmatrix}, \tag{124} $$

PREPRINT

Please cite and use: https://doi.org/10.1016/j.ymssp.2020.107168; contact authors if you need a copy.

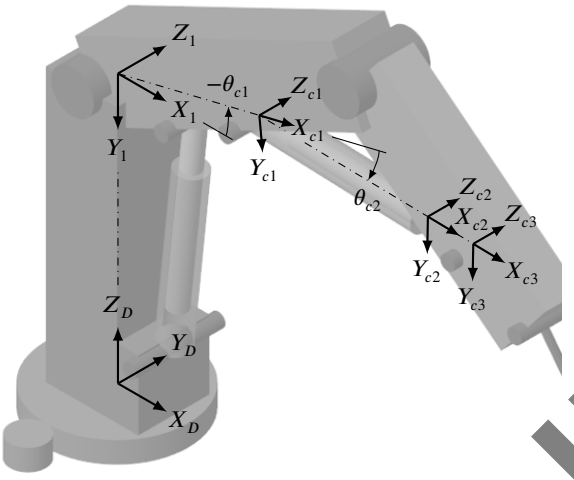

Figure 17: The coordinate frames for the jib actuator kinematic chain of the knuckle boom crane.

$$ {}^{c1}T_{c2} = \begin{bmatrix} c(\theta_{c2}) & -s(\theta_{c2}) & 0 & l_{c2}c(\theta_{c2}) \\ s(\theta_{c2}) & c(\theta_{c2}) & 0 & l_{c2}s(\theta_{c2}) \\ 0 & 0 & 1 & 0 \\ 0 & 0 & 0 & 1 \end{bmatrix}, \tag{125} $$

$$ {}^{c2}T_{c3} = \begin{bmatrix} 1 & 0 & 0 & d_2 \\ 0 & 1 & 0 & 0 \\ 0 & 0 & 1 & 0 \\ 0 & 0 & 0 & 1 \end{bmatrix}, \tag{126} $$

$$ {}^{c2}T_{CoG,c1} = \begin{bmatrix} 1 & 0 & 0 & -l_{CoG,c1} \\ 0 & 1 & 0 & 0 \\ 0 & 0 & 1 & 0 \\ 0 & 0 & 0 & 1 \end{bmatrix}, \tag{127} $$

$$ {}^{c3}T_{CoG,c2} = \begin{bmatrix} 1 & 0 & 0 & -l_{CoG,c2} \\ 0 & 1 & 0 & 0 \\ 0 & 0 & 1 & 0 \\ 0 & 0 & 0 & 1 \end{bmatrix}. \tag{128} $$

Concatenating the transformation matrices,

$$ \begin{aligned} {}^{D}T_{CoG,c1} &= \begin{bmatrix} {}^{D}R_{CoG,c1} & {}^{0}\mathbf{r}_{CoG,c1} \\ 0 & 1 \end{bmatrix} \\ &= {}^{D}T_1\,{}^{1}T_{c1}\,{}^{c1}T_{c2}\,{}^{c2}T_{CoG,c1}, \end{aligned} \tag{129} $$

$$ \begin{aligned} {}^{D}T_{CoG,c2} &= \begin{bmatrix} {}^{D}R_{CoG,c2} & {}^{0}\mathbf{r}_{CoG,c2} \\ 0 & 1 \end{bmatrix} \\ &= {}^{D}T_1\,{}^{1}T_{c1}\,{}^{c1}T_{c2}\,{}^{c2}T_{c3}\,{}^{c3}T_{CoG,c2}, \end{aligned} \tag{130} $$

and velocity matrices

$$ \begin{aligned} {}^{D}V_{CoG,c1} &= \begin{bmatrix} {}^{D}\tilde{\omega}_{CoG,c1} & {}^{D}\mathbf{v}_{CoG,c1} \\ 0 & 1 \end{bmatrix} \\ &= {}^{D}\dot{T}_{CoG,c1}\,{}^{D}T^{-1}_{CoG,c1}, \end{aligned} \tag{131} $$

PREPRINT

Please cite and use: https://doi.org/10.1016/j.ymssp.2020.107168; contact authors if you need a copy.

$$
\begin{aligned}
{}^{D}V_{CoG,c2} &= \begin{bmatrix} {}^{D}\tilde{\omega}_{CoG,c2} & {}^{D}\mathbf{v}_{CoG,c2} \\ 0 & 1 \end{bmatrix} \\
&= {}^{D}\dot{T}_{CoG,c2}\,{}^{D}T^{-1}_{CoG,c2}.
\end{aligned} \tag{132}
$$

D.1.4. Expressing Joint Angles in terms of Actuator Extensions

As the generalized coordinates were chosen to be $d_1(t)$ and $d_2(t)$, the joint angles $\theta_1(t)$ and $\theta_2(t)$ used in the kinematic equations, as well as angles $\theta_{b2}(t)$, $\theta_{c1}(t)$ and $\theta_{c2}(t)$ must be expressed in terms of $d_1(t)$ and $d_2(t)$. Using the geometry provided in Figure 8,

$$
\begin{aligned}
\theta_1(d_1(t)) =& \frac{\pi}{2} - \cos^{-1}\left(\frac{a_1^2 + b_1^2 - (d_1(t) + l_{b2})^2}{2a_1 b_1}\right) \\
&- \tan^{-1}\left(\frac{l_{b1x}}{l_0 - l_{b1z}}\right) - \tan^{-1}\left(\frac{l_{b4y}}{l_{b4x}}\right),
\end{aligned} \tag{133}
$$

$$
\begin{aligned}
\theta_2(d_2(t)) =& \pi - \cos^{-1}\left(\frac{a_2^2 + b_2^2 - (d_2(t) + l_{c2})^2}{2a_2 b_2}\right) \\
&- \tan^{-1}\left(\frac{l_{c1y}}{l_{c1x}}\right) - \tan^{-1}\left(\frac{l_{c3y}}{l_{c3x}}\right),
\end{aligned} \tag{134}
$$

$$
\begin{aligned}
\theta_{b2}(d_1(t)) =& \frac{\pi}{2} - \cos^{-1}\left(\frac{b_1^2 + (d_1(t) + l_{b2})^2 - a_1^2}{2b_1(d_1(t) + l_{b2})}\right) \\
&- \cos^{-1}\left(\frac{l_{b1x}}{b_1}\right),
\end{aligned} \tag{135}
$$

$$
\begin{aligned}
\theta_{c1}(d_1(t)) =& \tan^{-1}\left(\frac{l_{c1y}}{l_1 - l_{c1x}}\right) + \frac{\pi}{2} \\
&- \cos^{-1}\left(\frac{a_1^2 + b_1^2 - (d_1(t) + l_{b2})^2}{2a_1 b_1}\right) \\
&- \tan^{-1}\left(\frac{l_{b4y}}{l_{b4x}}\right) - \tan^{-1}\left(\frac{l_{b1x}}{l_0 - l_{b1z}}\right),
\end{aligned} \tag{136}
$$

$$
\begin{aligned}
\theta_{c2}(d_2(t)) =& \cos^{-1}\left(\frac{a_2^2 + (d_2(t) + l_{c2})^2 - b_2^2}{2a_2(d_2(t) + l_{c2})}\right) - \frac{\pi}{2} \\
&+ \tan^{-1}\left(\frac{l_{c1x}}{l_{c1y}}\right) - \tan^{-1}\left(\frac{l_{c1y}}{l_1 - l_{c1x}}\right),
\end{aligned} \tag{137}
$$

where

$$a_1 = \sqrt{l_{b4x}^2 + l_{b4y}^2}, \tag{138}$$

$$b_1 = \sqrt{l_{b1x}^2 + (l_0 - l_{b1z})^2}, \tag{139}$$

$$a_2 = \sqrt{l_{c1x}^2 + l_{c1y}^2}, \tag{140}$$

$$b_2 = \sqrt{l_{c3x}^2 + l_{c3y}^2}. \tag{141}$$

PREPRINT

Please cite and use: https://doi.org/10.1016/j.ymssp.2020.107168; contact authors if you need a copy.

D.1.5. Lagrangian

With the velocity matrices of each CoG defined, the kinetic energy K_i corresponding to link i can be calculated using

$$K_i = \frac{1}{2} m_i \left({}^{D}\mathbf{v}_i^T \cdot {}^{D}\mathbf{v}_i \right) + \frac{1}{2} {}^{D}\tilde{\omega}_i^T \, {}^{D}I_i \, {}^{D}\tilde{\omega}_i, \tag{142}$$

where ${}^{D}I_i$ is the inertia matrix of link i with respect to the deck coordinate frame,

$${}^{D}I_i = {}^{D}R_i I_i \, {}^{D}R_i^T, \tag{143}$$

where I_i is the inertia matrix of link i about its CoG. Note that for the slew motor,

$$K_a = \frac{1}{2} J_a N^2 \dot{\theta}_0^2, \tag{144}$$

where N is the gear ratio between the slew motor and the crane base. The potential energy P_i of link i can be expressed by

$$P_i = m_i \mathbf{g_D}^T \cdot {}^{D}\mathbf{r}_i. \tag{145}$$

The Lagrangian can then be calculated as

$$L = \sum_i K_i - \sum_i P_i, \tag{146}$$

where each sum is taken over all the links in the crane. The final equations of motion can then be found,

$$\frac{d}{dt}\left(\frac{dL}{d\dot{q}}\right) - \frac{dL}{dq} = F_q. \tag{147}$$

Using the six generalized coordinates given in equation (32), the equations of motion take the same form as for the five-DOF gantry crane,

$$\begin{bmatrix} M_{11} & M_{12} & M_{13} & M_{14} & M_{15} & M_{16} \\ M_{21} & M_{22} & M_{23} & M_{24} & M_{25} & M_{26} \\ M_{31} & M_{32} & M_{33} & M_{34} & M_{35} & M_{36} \\ M_{41} & M_{42} & M_{43} & M_{44} & M_{45} & M_{46} \\ M_{51} & M_{52} & M_{53} & M_{54} & M_{55} & M_{56} \\ M_{61} & M_{62} & M_{63} & M_{64} & M_{65} & M_{66} \end{bmatrix} \begin{bmatrix} \ddot{\theta}_0 \\ \ddot{d}_1 \\ \ddot{d}_2 \\ \ddot{l}_3 \\ \ddot{\theta}_3 \\ \ddot{\theta}_4 \end{bmatrix} + \begin{bmatrix} a_1 \\ a_2 \\ a_3 \\ a_4 \\ a_5 \\ a_6 \end{bmatrix} = \begin{bmatrix} -N\tau_a \\ F_b \\ F_c \\ F_l \\ 0 \\ 0 \end{bmatrix}. \tag{148}$$

The equations of motion for the knuckle boom crane are available as a supplementary file in MATLAB code. Note that the follow notation is used in the MATLAB code:

$$\frac{\partial \theta_1}{\partial d_1} = \text{dt\_1}, \tag{149}$$

$$\frac{\partial^2 \theta_1}{\partial {d_1}^2} = \text{ddt\_1}, \tag{150}$$

PREPRINT

Please cite and use: https://doi.org/10.1016/j.ymssp.2020.107168; contact authors if you need a copy.

$$\frac{\partial \theta_2}{\partial d_2} = \text{dt\_2}, \tag{151}$$

$$\frac{\partial^2 \theta_2}{\partial {d_2}^2} = \text{ddt\_2}, \tag{152}$$

$$\frac{\partial \theta_{b2}}{\partial d_{b2}} = \text{dt\_b2}, \tag{153}$$

$$\frac{\partial^2 \theta_{b2}}{\partial {d_{b2}}^2} = \text{ddt\_b2}, \tag{154}$$

$$\frac{\partial \theta_{c1}}{\partial d_{c1}} = \text{dt\_c1}, \tag{155}$$

$$\frac{\partial^2 \theta_{c1}}{\partial {d_{c1}}^2} = \text{ddt\_c1}, \tag{156}$$

$$\frac{\partial \theta_{c2}}{\partial d_{c2}} = \text{dt\_c2}, \tag{157}$$

$$\frac{\partial^2 \theta_{c2}}{\partial {d_{c2}}^2} = \text{ddt\_c2}, \tag{158}$$

$$\dot{\theta}_0 = \text{t\_0dot}, \tag{159}$$

$$\dot{d}_1 = \text{d\_1dot}, \tag{160}$$

$$\dot{d}_2 = \text{d\_2dot}, \tag{161}$$

$$\dot{l}_3 = \text{l\_3dot}, \tag{162}$$

$$\dot{\theta}_3 = \text{t\_3dot}, \tag{163}$$

$$\dot{\theta}_4 = \text{t\_4dot}, \tag{164}$$

$$\Theta_r = \text{t\_r}, \tag{165}$$

$$\Phi_p = \text{t\_p}. \tag{166}$$

Any terms with subscripts are written with an underscore (for example, l_0 is replaced with l_0).

CRediT authorship contribution statement

Iain A. Martin: Methodology, Software, Validation, Formal analysis, Writing - Original Draft, Visualization. **Rishad A. Irani:** Conceptualization, Resources, Investigation, Data Curation, Writing - Review & Editing, Supervision, Project administration, Funding acquisition.

References

[1] Agostini, M., et al., 2002. Command shaping and closed-loop control interactions for a ship crane, in: Proceedings of the American Control Conference, Anchorage, AK.

[2] Chu, Y., et al., 2014. An effective heave compensation and anti-sway control approach for offshore hydraulic crane operations, in: Proceedings of the 2014 IEEE International Conference on Mechatronics and Automation.

[3] DSA-Ltd, . Shipmo3d. [Online]. Available: `https://dsa-ltd.ca/shipmo3d/overview/`. [Accessed: 19-Aug-2019].

[4] Fang, Y., Wang, P., 2012. Advanced nonlinear control of an offshore boom crane, in: 2012 American Control Conference (ACC).

[5] Fang, Y., et al., 2014. Dynamics analysis of nonlinear control of an offshore boom crane. IEEE Transactions on Industrial Electronics 61(1), 414–426.

[6] Frikha, S., Djemel, M., Derbel, N., 2018. A new adaptive neuro-sliding mode control for gantry crane. International Journal of Control, Automation and Systems 16(2), 559–565.

[7] Guo, B., Chen, Y., 2020. Fuzzy robust fault-tolerant control for offshore ship-mounted crane system. Information Sciences (Pre-proof) .

[8] Henry, R., et al., 2001. Cargo pendulation reduction on ship-mounted cranes via boom-luff angle actuation. Journal of Vibration and Control 7(1), 1253–1264.

[9] Ismail, R., Ha, Q., 2013a. Trajectory tracking and anti-sway control of three-dimensional offshore boom cranes using second-order sliding modes, in: 2013 IEEE International Conference on Automation Science and Engineering (CASE).

PREPRINT

Please cite and use: https://doi.org/10.1016/j.ymssp.2020.107168; contact authors if you need a copy.

[10] Ismail, R., Ha, Q., 2013b. Trajectory tracking control for offshore boom cranes using higher-order sliding modes, in: Proceedings of the International Symposium on Automation and Robotics in Construction (ISARC).
[11] Ismail, R., That, N., Ha, Q., 2015. Modelling and robust trajectory following for offshore container crane systems. Automation in Construction 59, 179–187.
[12] Jazar, R., 2010. Theory of Applied Robotics. Springer.
[13] Kim, D., Park, Y., 1999. Tracking control in x-y plane of an offshore container crane. Trans. of the Society of Instrument and Control Engineers 35(2), 253–261.
[14] Kim, G., Hong, K., 2019. Adaptive sliding mode control of an offshore container crane with unknown disturbances. IEEE/ASME Transactions on Mechatronics .
[15] Lu, B., Fang, Y., Sun, N., 2019. Nonlinear coordination control of offshore boom cranes with bounded control inputs. International Journal of Robust Nonlinear Control 29, 1165–1181.
[16] Lu, B., et al., 2018. Antiswing control of offshore boom cranes with ship roll disturbances. IEEE Transactions on Control Systems Technology 26(2), 740–747.
[17] Maghsoudi, M., et al., 2019. Improved unity magnitude input shaping scheme for sway control of an underactuated 3d overhead crane with hoisting. Mechanical Systems and Signal Processing 123, 466–482.
[18] Martin, I., Irani, R., 2019. Evaluation of both linear and non-linear control strategies for a shipboard marine gantry crane, in: Oceans Seattle 2019.
[19] Masoud, Z., Nayfed, A., Mook, D., 2004. Cargo pendulation reduction of ship-mounted cranes. Nonlinear Dynamics 35, 299–311.
[20] Ngo, Q., Hong, G., Hong, K., 2011. Sway suppression of an offshore container crane. 2011 IEEE/SICE International Symposium on System Integration .
[21] Ngo, Q., Hong, K., 2012. Sliding-mode antisway control of an offshore container crane. IEEE/ASME Transactions on Mechatronics 17(2), 201–209.
[22] Ngo, Q., et al., 2017. Fuzzy sliding mode control of an offshore container crane. Ocean Engineering 140, 125–134.
[23] Nguyen, N., Ngo, Q., Ha, Q., 2015. Active control of an offshore container crane. 2015 International Conference on Control, Automation and Systems (ICCAS) .
[24] Qian, Y., Fang, Y., Lu, B., 2015. A learning strategy based partial feedback linearization control method for an offshore boom crane, in: 2015 IEEE Annual Conference on Decision and Control (CDC).
[25] Qian, Y., Fang, Y., Lu, B., 2017. Adaptive repetitive learning control for an offshore boom crane. Automatica 82, 21–28.
[26] Qian, Y., Fang, Y., Lu, B., 2019. Adaptive robust tracking control for an offshore ship-mounted crane subject to unmatched sea wave disturbances. Mechanical Systems and Signal Processing 114, 556–570.
[27] Ramli, L., Mohamed, Z., Jaafar, H., 2018. A neural network-based input shaping for swing suppression of an overhead crane under payload hoisting and mass variations. Mechanical Systems and Signal Processing 107, 484–501.
[28] Ramli, L., et al., 2017. Control strategies for crane systems: A comprehensive review. Mechanical Systems and Signal Processing 95, 1–23.
[29] Ramli, L., et al., 2020. Efficient swing control of an overhead crane with simultaneous payload hoisting and external disturbances. Mechanical Systems and Signal Processing 135, 106326.
[30] Singh, A., Agrawal., H., 2018. A fractional model predictive control design for 2-d gantry crane system. Journal of Engineering Science and Technology 13(7), 2224–2235.
[31] Spathopoulos, M., Fragopoulos, D., 2004. Pendulation control of an offshore crane. International Journal of Control 77(7), 654–670.
[32] Sun, N., et al., 2018. Nonlinear antiswing control of offshore cranes with unknown parameters and persistent ship-induced perturbations: Theoretical design and hardware experiments. IEEE Transactions on Industrial Electronics 65(3), 2629–2641.
[33] Sun, N., et al., 2019. Dynamic feedback antiswing control of shipboard cranes without velocity measurement: Theory and hardware experiments. IEEE Transactions on Industrial Informatics 15(5), 2879–2891.
[34] Suthakorn, J., Parker, G., 2005. Anti-swing control of suspended loads on shipboard robotic cranes. Journal of Systemics, Cybernetics and Informatics 3(1), 35–40.
[35] Tysse, G., Egeland, O., 2018. Dynamic interaction of a heavy crane and a ship in wave motion. Modeling, Identification and Control 39(2), 45–60.
[36] Wang, S., et al., 2018. Dynamic modelling and analysis of 3-axis motion compensated offshore cranes. Ships and Offshore Structures 13(3), 265–272.
[37] Yang, T., et al., 2019. Neural network-based adaptive antiswing control of an underactuated ship-mounted crane with roll motions and input dead zones. IEEE Transactions on Neural Networks and Learning Systems Ahead of Print.
[38] Yao, B., Bu, F., Chiu, G., 2001. Non-linear adaptive robust control of electro-hydraulic systems driven by double-rod actuators. International Journal of Control 74(8), 761–775.
[39] Zhang, Z., Li, L., Wu, Y., 2018. Disturbance-observer-based antiswing control of underactuated crane systems via terminal sliding mode. IET Control Theory and Applications 12(18), 2588–2594.
[40] Zodiac-Nautic.com, . Open 6.5. [Online]. Available: https://www.zodiac-nautic.com/en/shop/produits/boats/open-en/open-6-5. [Accessed: 15-Mar-2019].

PREPRINT